AQRP Final Report

Quantifying the Emissions and Spatial/Temporal Distributions of Consumer Volatile Chemical Products (VCPs) in the Greater Houston Area

AQRP Project 22-020

Submitted by

Dr. Yue Zhang
Dr. Qi Ying
Texas A&M University

Executive Summary

This report focuses on characterizing the concentration and spatial distributions of volatile chemical products (VCPs) in the Greater Houston Areas (GHA) using the Texas A&M mobile lab. The VCPs consist of volatile organic compounds (VOCs) produced from consumer products and business activities, including personal care products, printing inks, pesticides, cleaning agents, and organic coatings. Houston has no reported ambient measurements of the VCP to our knowledge, highlighting the urgent need to characterize VCP concentration in the Greater Houston Area validated by ambient measurements with detailed spatial and temporal resolution. Such data will improve understanding of the VCPs in an important area of Texas where there are complicated emissions from tailpipes, industrial, and residential usage, to provide information that can curb future VCO emissions.

The mobile lab was equipped with a Vocus 2R Chemical Ionization Time-of-Flight Mass Spectrometer (CIMS), High-Resolution Time-of-Flight Aerosol Mass Spectrometer (HR ToF AMS), ozone monitor, CO monitor (PICARRO G2401), aethalometer, scanning electrical mobility sizer (SEMS), RH monitor, temperature sensor, and VK172 G-Mouse USB GPS Receiver. Ambient air was supplied to the instruments at a total flow rate of 5 liters per minute (LPM).

A modified version of the Community Multiscale Air Quality (CMAQ) model was updated to use the detailed version of the SAPRC-11 photochemical mechanism (SAPRC-11D) to determine the concentrations of volatile chemical products (VCPs) in the Houston area. The SAPRC-11 chemical mechanism is the updated version of the widely used SAPRC-07 chemical mechanism. The SAPRC-11D differs from other versions of the SAPRC mechanism by explicitly representing the oxidation of a large number of precursor VOCs and it was shown to outperform the lumped SAPRC-11L mechanism in predicting O_3 concentrations in the Houston area (AQRP project 12-006). The SAPRC-11D has been used for SOA modeling in the US and China.

During the funded period, we have performed three field campaigns in total, exceeding the original one field campaign proposed in the original proposal and two field campaigns in the revised proposal. These campaigns cover the emissions and concentrations of VCPs in summer, fall, and winter seasons. Our results show that the concentrations of seven major VCP groups, namely acetone, PCBTF from solvent-based coating emissions, D5-siloxane from personal care products, D4-siloxane from adhesives and insecticides, monoterpenes from fragrances, methyl ethyl ketone (source), and texanol from water-based coatings and adhesives. The concentrations of these VCPs range from <0.1 ppt for PCBTF and Texanol to 1-7 ppb for acetone. Monoterpene shows strong seasonal differences in their concentrations, while the concentrations of other types of VCP during different seasons remain to be statistically the same. It is expected that monoterpene has a more drastic seasonal difference due to biogenic emissions during the summer and fall. Our data further shows that the VCP concentrations measured by the experiments are higher than modeling output, sometimes even significantly higher than modeling results, suggesting that current CAMQ model and national inventory may underpredict the ozone formation. Further studies using updated VCP reaction scheme and inventories developed by the TCEQ is needed to more accurately quantify and model VCP and ozone concentrations in Houston.

The results of this study have so far generated two first-author manuscripts under preparation, and one more relevant manuscript ready to be submitted to the Science magazine which the PI Zhang's team serves as a coauthor on.

1 Introduction

1.1 Background

Air pollution is the fifth largest cause of death in the world. Volatile organic compounds (VOCs) can also undergo chemical reactions with atmospheric oxidants to form major atmospheric pollutants, such as particulate matter (PM) and photochemically generated ozone (O_3). Traditionally, a significant portion of the urban VOC comes from urban vehicle and tailpipe emissions. During the past few decades, VOC emissions from tailpipe emissions have been significantly reduced, leading to an increase of the contribution of other types of VOCs. In urban areas, the volatile chemical products (VCPs) have become an important sources of anthropogenic VOCs.

VCPs consist of VOCs produced from consumer products and business activities, including personal care products, printing inks, pesticides, cleaning agents, and organic coatings. Emissions of VCPs are dominated by oxygenated compounds, alkanes (such as acetone, isopropyl alcohol, propane, and isobutane), and personal care products (such as D5-siloxane and monoterpenes). Recent studies have shown that VCPs account for up to half of the petrochemical VOCs in urban areas, which is comparable to or exceeding the emissions of a summer forest. However, there are significant variations in the spatial and temporal distributions of VCPs among different urban areas.

Currently, the emissions of VCPs from residential, commercial, institutional, and industrial sources have been included in the National Emissions Inventory (NEI) as the solvent utilization sector.[4] The current NEI inventory highlights an increasing relative importance of VCP in VOC emissions within the state of Texas. Nevertheless, the community now needs measurement data to validate such emission sources. For instance, the NEI inventory might still be lower than the actual concentrations. McDonald et al. showed that the VCP emissions at Los Angeles based on NEI might be a factor of 2-3 lower. Seltzer et al. developed a new VCP emission inventory (VCPy) where they show an additional increase in VCP emission. The estimated 2017 VCP emissions in Texas from the VCPy inventory is 247 Gg, almost 20% higher than the NEI estimation of 212 Gg.

1.2 Measurement Need for VCP

As the fourth largest city in the US with more than 7 million people in the Greater Houston Areas (GHA), Houston has no reported ambient measurements of the VCP to our knowledge, highlighting the urgent need to characterize VCP concentration in the Greater Houston Area validated by ambient measurements with detailed spatial and temporal resolution. Such data will improve understanding of the VCPs in an important area of Texas where there are complicated emissions from tailpipes, industrial, and residential usage, to provide information that can curb future VCO emissions.

1.3 Modeling Need for VCP

In addition, personal care products, one of the major VCP ingredients, may significantly contribute to O_3 formation due to their double bond structure.[15] These personal care products often contain fragrances such as monoterpenes, which can readily react with atmospheric oxidants such as OH, NO_3, and O_3 due to their double bond structure, thus having relatively short atmospheric lifetimes compared with alkanes from vehicle emissions and other types of VCPs.For instance, Coggon et al. shows that emission of anthropogenic monoterpene in New York City is 14.7-24.4 kg d^{-1} km^{-2}, similar to the summertime monoterpene emissions for a typical forest in the United States. Since

the O_3 formation in the urban areas are mostly VOC-limited, VCPs account for more than half of the 20 ppb maximum daily average 8-h (MDA8) O_3 attributed to anthropogenic VOCs. Previous study demonstrates that oxygenated VOCs from the VCPs (oVCPs) could cause 15-20% of increase in peroxyacetyl nitrate (PAN) concentrations compared to oVCPs comprised of hydrocarbons. The higher concentrations of PAN may cause enhanced O_3 formation in downwind areas. In addition, VCP-derived SOA can also contribute to half of the background SOA in Los Angeles and significantly reduce the bias of ozone and PM mass concentration predicted by models.

1.4 Our Proposed Research Objectives

Hence, we propose to carry out three major objectives. **(1)** conduct field measurements of a broad range of VOCs, including oxygenated VOCs and monoterpenes, in the Greater Houston area using the Vocus Chemical Ionization Time-of-Flight Mass Spectrometer (Vocus CI-MS) on a mobile platform; **(2)**characterize seasonal difference of VCP concentrations in Houston; and **(3)** improve understandings of how VCP affect air quality in the Houston$_3$. We have made significant progress in these areas with the results shown in this report by integrating laboraotry calibration, field measurements, with up-to-dated models.

1. Methods and Techniques

For this study, we conducted field measurements of a broad range of VOCs, including oxygenated VOCs and monoterpenes, in the Greater Houston area (GHA) using the Vocus Chemical Ionization Time-of-Flight Mass Spectrometer (Vocus CI-MS) on a mobile platform. We characterize seasonal and spatial differences of VCPs and organic aerosol concentrations in the GHA. Specifically, the Texas A&M University Rapid Measurements Van (TRAM van) was deployed to measure the urban atmospheric composition across the GHA. The TRAM van includes a Vocus 2R Chemical Ionization Mass Spectrometer (Vocus 2RCI-MS), SP-HR-ToF-AMS, carbon monoxide (CO) monitor, Scanning Electrical Mobility Sizer (SEMS), and relative humidity (RH), temperature, and GPS monitors.

Temporal, seasonal, and spatial measurements were taken over the course of this project. Field campaigns were performed during the late summer/fall and in the winter to understand the seasonal trend of VCPs in the GHA. We collected 7 days of data in the fall and 11 days in the winter. During the field campaigns, 3 different routes were done around the GHA to obtain a thorough spatial dataset. Each route took ~8 hours, so data was collected over a large timeframe during the day.

During the field campaign, we used two different ionization methods for the Vocus-CIMS including PTR (H+) mode and ammonium (NH4+) mode. Doing this allowed us to identify which mode best detects each VCP compound. We used each ionization method at least once for each route and each season.

The Vocus CI-MS data collected from the Fall and Winter time periods were analyzed to compare the VCP composition, concentration, and spatial distributions to understand the differences of VCPs in the ambient environment between summertime and wintertime in the GHA. Included in this report are measurements of common tracer VCP species. These include measurements of common solvents, such as acetone, PCBTF from solvent-based coating emissions, D5-siloxane from personal care products, D4-siloxane from adhesives and insecticides, monoterpenes from fragrances, methyl ethyl ketone (source), and texanol from water-based coatings and adhesives. Table 2 shows the VCPs reported for this report. We also analyze the impact of traffic-related

VOC compounds on total VOC emissions by examining VOC:CO ratios obtained from ambient measurements.

The HR-ToF-AMS data collected from the Fall and Winter time periods were analyzed to compare the organic aerosol composition, concentration, and spatial distributions to understand the differences in organic aerosols in the ambient environment between summertime and wintertime in the GHA. Included in this report are measurements of total organic concentrations of aerosols and inorganic concentrations including chlorine, NH4, NO3, and SO4.

Data with carbon monoxide concentration (CO) was analyzed to understand the impact of mobile sources on VCP emissions. We estimate VOC emissions from mobile sources by evaluating the VOC:CO mixing ratios measured during the field campaign. Additionally, we look at correlation between different VCPs and CO to identify any notable time periods where the air masses over the GHA were stagnant, resulting in high correlation between VCPs and CO mixing ratios.

Table 2.1. List of VCPs measured in this study

Compound	**Formula**	**m/z**	**m/z H^+ add-on**	**m/z NH_4^+ add-on**
Acetone	C_3H_6O	58.08	59.08	76.08
Methly Ethyl Ketone (MEK)	C_4H_8O	72.11	73.11	90.15
D4-Siloxane	$C_8H_{24}O_4Si_4$	296.08	297.08	314.12
D5-Siloxane	$C_{10}H_{30}O_5Si_5$	370.10	371.10	388.14
Monoterpenes	$C_{10}H_{16}$	136.13	137.13	154.17
PCBTF	$C_7H_3ClF_2$	159.996	160.996	177.996
Texanol	$C_{12}H_{24}O_3$	216.317	217.317	234.317

2.1 Measurement Instruments and Schematic Graphs

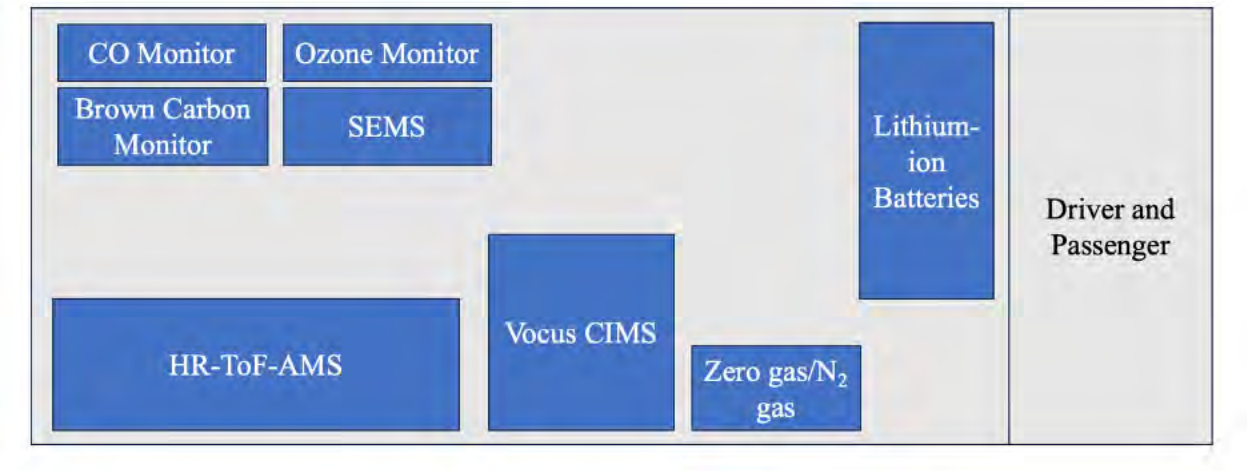

Figure 2.2. Schematic of the Texas A&M University Rapid Measurements Van (TRAM van) instrument setup

The mobile lab was equipped with a Vocus 2R Chemical Ionization Time-of-Flight Mass Spectrometer (CIMS), High-Resolution Time-of-Flight Aerosol Mass Spectrometer (HR ToF AMS), ozone monitor, CO monitor, SMPS, RH monitor, and temperature monitor. Ambient air was supplied to the instruments at a total flow rate of 5 liters per minute (LPM).

Time series of size distribution and total volume concentration data of ambient particles were generated with Scanning Electrical Mobility Sizer (SEMS). Temperature and relative humidity were measured using an OMEGA RH sensor. GPS coordinates were measured using a VK172 G-Mouse USB GPS Receiver for Windows.Time series of CO concentrations were measured using a PICARRO G2401 Gas Concentration Monitor

Table 2.2 Examples of instruments, data, and inferences

Instrument	Parameter	Data
SP-HR-ToF-AMS	peak area	VCP-derived Particle mass loading. The quantification of the VCP mass loading can be used to understand how much VCP can be oxidized in the atmosphere to form aerosols.
HR-ToF-Vocus CIMS Instruments	peak area	VCP concentration. The quantification of VCP can be used to calculate VCP emissions and chemical transformations in the atmosphere.
Aethalometer	Optical sensor signal	Total black carbon and brown carbon measured during selected time intervals
CO analyzer	Instrument peak area	CO concentration measured from the gas phase
NO_2 analyzer	Optical sensor signal	NO_2 concentration measured from the gas phase
Filters	Mass spectrometer signals	Organic species detected on the filters

2.2 Working Principles of Major Instrument

Time series of chemical composition and mass spectra were generated with the Vocus-CIMS instrument. The Vocus CIMS ionizes the gaseous analyte via gas-phase ion–molecule reactions. In this study, we used 2 ionization methods including PTR (H+) and ammonium (NH4+). The Vocus uses a quadrupole RF field in the reactor to collimate ions onto the central axis and improve the detection limit, while maintaining similar collision conditions for conventional drift tubes in the meantime. The reagent-ion source consists of two conical surfaces between which a plasma is produced. The corresponding vapor will enter the focusing ion-molecule reactor (FIMR). The discharged current is regulated to be 1.5 – 2.0 mA. The sampling air will enter the FIMR with a pressure of 1 mbar, which is controlled by a valve between the reactor and a mechanical pump. The FIMR consists of a 10 cm glass tube and a homogeneous electric field will be generated. At the end of the FIMR, the adduct ions are sampled into a time-of-flight mass spectrometer for

detection. The ions from FIMR first enter a big, segmented quadrupole (BSQ) region to focus the ion beam, and then enter the primary beam (PB) region, and finally the ToF chamber. The BSQ acts as a high-pass band filter that ions smaller than specific mass-to-charge ratio (m/z) determined by the voltage setting will be detected at a much lower efficiency. Such setting could help prevent the degradation of the microchannel plate detector due to the very high reagent ion intensities.

Time series of non-refractory submicron aerosol composition was generated with the HR-ToF-AMS. The AMS consists of three main sections, including the aerosol sampling chamber, particle sizing chamber, and particle composition detector chamber. In the aerosol sampling chamber, the AMS has an aerodynamic lens coupled with the vacuum that will focus the aerosol into a narrow beam from the atmospheric air samples. The narrow beam is approximately 1 mm in diameter and particle transmission efficiency to the detector of nearly 100% for the particle size range of 70 to 500 nm. The focused beam exiting the sampling chamber is directed to the particle sizing chamber. The particle sizing chamber is maintained at approximately 105 torr by a 550 L/s turbo pump. The particles are directed in this chamber through a skimmer cone and the aerosol beam is modulated in this chamber by a rotating wheel chopper. The aerodynamic diameter is obtained from particle velocity, which is given by time-resolved detection of particles coupled with known flight distance. Particles with different sizes will travel at different speeds after the chopper and are focused into the detection chamber. The particle detection chamber is isolated from the sizing chamber by an aperture with 4 mm diameter. A molecular turbo pump is used to pump this chamber differentially at 250 L/s. A diaphragm pump operating at inlet pressure of 1.2 torr and 60 L/min is used to back the turbo pump of the particle detection chamber. The particles are directed to a resistively heated close end tube, where semivolatile/volatile constituents in the particle vaporize at 600 °C. The vaporized gasses are then ionized with an electron beam of 70 eV using the electron impact ionization method. After the ionization, the ion fragments will be analyzed using a quadrupole mass analyzer. The instrument is connected to the computer system for data acquisition which processes the data in real time.

2.3 Deployment Schedule and Map

Fall and winter field deployments were performed beginning in October 2022 and ending in January 2023. We additionally plan to complete a summer field campaign in August 2023. The first campaign began on October 30th and ended on November 9th. We obtained VCP, CO, and organic aerosol data on 7 days including 10/30, 11/2, 11/4, 11/5, 11/6, 11/7, and 11/9. The second campaign began on January 12th and ended on January 24th. We obtained VCP, CO, and organic aerosol data on 11 days including 1/12, 1/13, 1/14, 1/15, 1/17, 1/18, 1/19, 1/21, 1/22, 1/23, and 1/24. For the summer campaign, we plan to collect data for 6 days from August 1st to August 10th.

During the campaigns, we performed three different routes to obtain measurements with a large spatial resolution of the Houston metro area. All routes began and ended at the University of Houston located at 4701 Martin Luther King Blvd, Houston, TX 77004 as highlighted in figure 2.3. For all three routes, major highways and interstates were avoided, when possible, to limit the influence of vehicle emissions. The first route circled around I-610 and the downtown area as shown in figure 2.3a. The second route went East-West moving parallel to I-10 as shown in figure 2.3b. The last and third route went North-South moving parallel to I-45 as shown if figure 2.3c.

We used ammonium mode during 10/30, 11/2, and 11/4 and PTR mode for 11/5, 11/6, 11/7, and 11/9 for the fall campaign. Similarly, we used ammonium mode during 1/12, 1/13, 1/14, and 1/15

and PTR mode for 1/17, 1/18, 1/19, 1/21, 1/22, 1/23, and 1/24. Table 2 shows a detailed discussion of the ionization mode and route for each deployment day.

Table 2: Summary of each deployment day including route and ionization methods

Fall			**Winter**		
Date	Route	Ionization Mode	Date	Route	Ionization Mode
10/30	Round	NH_4^+	1/12	North South	NH_4^+
11/02	East West	NH_4^+	1/13	Round	NH_4^+
11/04	Round	NH_4^+	1/14	Round	NH_4^+
11/05	North South	H^+	1/15	East West	NH_4^+
11/06	Round	H^+	1/17	Round	H^+
11/07	Round	H^+	1/18	Round	H^+
11/09	East West	H^+	1/19	North South	H^+
			1/21	East West	H^+
			1/22	North South	H^+
			1/23	Round	H^+
			1/24	North South	H^+

Figure 2.3 shows the three typical routes for the mobile deployment

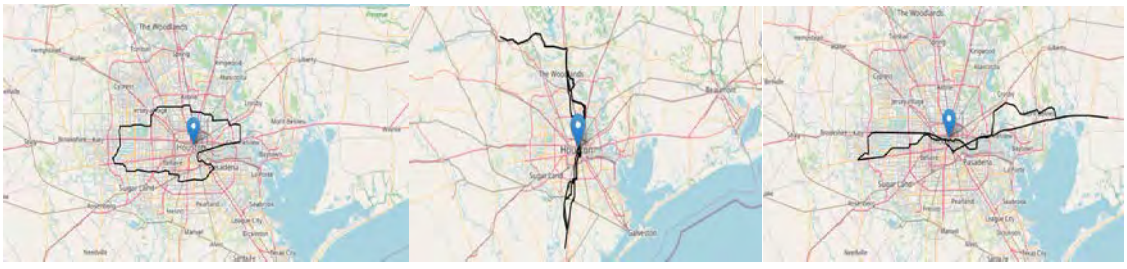

Figure 2.3: Map highlighting each of three routes. The blue marker shows University of Houston

2.4 Data Collection Protocol

Data were collected using all the instruments described above from the mobile laboratory. The collection procedures are described below:

Field Measurements Quality Insurance:

During the field campaign, the van was driven under 30 mph to ensure that the ambient air was properly entering the inlet located on the top of the van. Additionally, major highways and interstates were avoided, when possible, to avoid significant tailpipe emissions from impacting the data. During each deployment, the instruments were monitored inside the van to ensure they were functioning properly.

Data acquired from all instruments was saved on a hard drive during the field deployments and backed up to the cloud service. Similarly, at the end of each deployment, data was copied from all instruments and inspected to ensure that the instruments were functioning properly.

HR-ToF-Vocus CIMS:

The gas-phase VCPs were sampled by the HR-ToF-Vocus CIMS instruments. For the HR-ToF-Vocus CIMS instruments, we first calibrated the instruments based on procedures described later in of this document. Once calibration was completed, ambient air was introduced into HR-ToF-Voucus CIMS instruments at a flow rate between 1-2 liters per minute (LPM). This instrument was operated between 10-35 °C and the relative humidity of the sample was controlled to be less than 60%. Two different ionization schemes, as described later, were used to sample the gas-phase VCPs depending on their sensitivity within each method.

The quality control of Vocus CIMS data included the following steps. Firstly, before the sampling, the calibration procedure as described below was performed. Secondly, prior to daily sampling, while the Vocus was sampling ambient air, the obtained mass spectrum should have specific ions as the highest. After the experiments, the data analysis of Vocus was performed using the Tofware package (version 3.2.3) running in the Igor Pro. The status of the instrument was examined during the data processing, and any bad data points based on the benchmark values were removed from the data set. Data cleaning was performed to remove all potential contaminated field data. For instance, when the instrument status is fluctuating due to the mobile lab vibration, environment temperature change, etc.

HR-ToF-Vocus CIMS Calibration:

The Vocus CIMS ionization efficiency calibration was done every hour during the field campaign with a calibration gas cylinder including ethanol, acetonitrile, acetone, acrylonitrile, isoprene, methyl vinyl ketone, methyl ethyl ketone, benzene, m-xylene, α-pinene, 1,2,4-trimethylbenzene, octamethylcyclotetrasiloxane, decamethylcyclopentasiloxane, and β-caryophyllene. The calibration gases are around 1000 ppb in the cylinder and were diluted into VOC-free air produced by a zero-air generator to around 10 ppb. The diluted calibrants were measured by the Vocus CIMS, and the sensitivity factor for each compound was derived with the unit cps (count per second)/ppb. First, zero air was injected at 300 sccm for 3 minutes, then, the calibration gas was injected at 5 sccm for 2 minutes. Changes in instrument sensitivity were accounted for by performing a linear regression between each hourly calibration point.

SP-HR-ToF-AMS:

AMS sampled particle-phase organic aerosols in real time. The aerosol samples were directed to AMS using conductive tubing to minimize particle loss. A flow meter was used to measure the inline flow to AMS to ensure the flow rate was between 1-2 LPM to reduce particle loss in the tubing. The instrument only takes 0.3 LPM of sample while the rest of the air samples go to the exhaust. The air sample was controlled to be less than 60% RH and the operating environment

temperature of the instrument was between 10-35 °C. We regularly monitored all the voltages and pressures inside the instrument throughout the campaign to ensure that they reached the setpoints.

The quality control of AMS data includes the following steps. Firstly, before the operation, calibration procedures were performed. Briefly, IE calibration was performed at an interval of two weeks. Flow rate calibration was performed along with the IE calibration every two week. Particle time of calibration was performed if the chopper wheel is perturbed or if there is a shift in vaporizer. Secondly, during the operation, m/z calibration was performed once daily before starting the analysis. Thirdly, after the deployment days, the data was imported into the PIKA Igor analysis software, where the flow rate and all voltages of the instrument during the operational period were examined. We identified any bad data points based on these benchmark values and removed them from the analysis software.

AMS: IE calibration.

An atomizer was used to generate the aerosols of ammonium sulfate/nitrate which was followed by a diffusion dryer. The aerosols generated were made monodisperse by passing them through differential mobility analyzer (DMA). After this, the fraction of aerosols was sampled by the AMS and condensation particle counter (CPC). The aerosols were analyzed at a minimum of five concentrations. The aerosol concentration was controlled by the dilution system installed before the AMS and the CPC. This method was used to calibrate the particle size dependent TOF measurement, to determine the particle collection or particle detection efficiency of the AMS. The IE calibration was carried out every two weeks. The acquired data was analyzed using IGOR software to generate calibration curves.

AMS: M/z calibration.

The mass calibration (m/z) of the instrument was carried out once daily before the start of deployment. The m/z calibration is done automatically by the data acquisition software when sampling. Generally, the ion peaks by N2, O2 and W are used for the m/z calibration. The N2 peak is the largest peak at m/z 28 followed by the O2 peak at m/z 32. Opposed to the ambient ion peak of N2 and O2, W ion peak at m/z 184 is caused by the heating material in the instrument. It is included to ensure validity for higher m/z values. From the m/z calibration panel of the software we can also follow peak properties like peak shape, peak intensity, and peak position.

AMS: Particle time of flight calibration.

Particle time of flight calibration of the instrument is done done only if the instrument is moved to a new measurement site (such as from laboratory to field campaign), if the chopper wheel is perturbed or there is a shift in position of the vaporizer. In the calibration procedure the PSL spheres of diameter generally in the range of 50 nm to 1000 nm are atomized and are passed through a diffusion dryer. The particles are monodispersed using DMA prior to AMS sampling and are sampled one diameter at a time. The instrument is run in the PTOF mode, and the acquired data is analyzed using IGOR software.

2.5 Data Analysis Procedures

The data analysis procedures for each instrument are described below. We keep the same procedures for each instrument to keep a consistent manner.

HR-ToF-Vocus CIMS:

HR-ToF-CIMS and Vocus 2R CIMS data were initially written into HDF5 files. Raw HDF5 files were imported into Tofware, an Igor-based software package, for data browsing and visualization, mass calibration, and high-resolution-peak fitting in batch operation. Raw HDF5 files are first averaged over 10 second time periods, which results in a new averaged HDF5 file.

The analyzed data by Igor are stored as a packed experiment (*.pxp) file. First, the averaged files are opened in batch mode. Then, the mass calibration is done for the entire time series by selecting at least five ions ranging from 0 to 400 m/z depending on the ionization mode for a gaussian peak shape. Next, a reference spectrum is defined typically using the mass of alpha-pinene. Then the baseline is refined. After this, the peak shape and width are defined. Then the mass calibration is done again to obtain a custom shape for each peak. Then specific ions are assigned to peaks ranging from 0-400 m/z, which includes all the VCP compounds. Finally, the files are batch fitted and integrated.

Peaks were assigned based on the ionization mode utilized during each campaign. Peaks were analyzed at each m/z to determine if there was any fragmentation of the analyte molecules during ionization by the Vocus CIMS. The two ionization methods used resulted in varying levels of fragmentation. This is the case because PTR mode is more likely to fragment analytes compared to ammonium mode. For the 7 VCP compounds identified in this report, Texanol was the only compound to exhibit significant fragmentation. Therefore, when using ammonium mode, we report time series data for the full molecule ($C_{12}H_{24}O_3$), but for PTR mode, we report time series data for the fragment ($C_{12}H_{22}O_2$). This is the case for all deployment days.

After the files were analyzed, time series of VOCs were obtained. For those in the calibration gas (ethanol, acetonitrile, acetone, acrylonitrile, isoprene, methyl vinyl ketone, methyl ethyl ketone, benzene, m-xylene, α-pinene, 1,2,4-trimethylbenzene, octamethylcyclotetrasiloxane, decamethylcyclopentasiloxane, and β-caryophyllene), calibration peaks are linearly interpolated to account for slight changes in instrument sensitivity that can occur from movement while driving. The linear interpolations are used to correct the data in between each calibration point.

Calibration curves were created from VCP standards for PCBTF, Texanol, and D4-siloxane to determine their specific detection limits in the Vocus-CIMS. This process will be repeated for the other VCP 50 compounds measured in this study. A Liquid Calibration System was attached to the Vocus-CIMS in order to run trials to produce the calibration curves. The solution used for calibration contained alpha-pinene, D4-siloxane, PCBTF, and Texanol, all at a 200 uM concentration. While running the trials, the gas flow rate was kept constant, and the liquid flow rate was adjusted at specific increments. Using these specific flow rates, as well as the concentration of the solution, the ideal gas law was applied to eventually reach a volume of gas containing the compounds listed above. This volume was then divided by the volume of gas flowing through the Vocus-CIMS from the gas flow rate to get a ppb concentration of each compound at each flow rate. In order to make the gas concentration more exact, the ratio of the proposed mass of a compound in the solution to the actual mass was applied to each ppb calculation. With the average ions per second for each flow rate and the ppb at each flow rate, a calibration curve was made, with ions per second on the y-axis and ppb on the x-axis. These calibration curve were linearly interpolated, and the ratio between the slope of the compound and the slope of alpha-pinene was used to correct the raw data.

After all corrections were completed, time series for acetone, MEK, monoterpenes, D4-siloxane, D5-siloxane, PCBTF, and texanol were obtained and averaged every minute as seen in section 4.1.

SP-HR-ToF-AMS:

SP-HR-ToF-AMS data are initially saved as HDF5 (Hierarchical Data Format) files. The AMS data obtained from the field campaign was analyzed using the data analysis software IGOR. Raw data are imported into Igor Pro (Wave Metrics) using SQUIRREL and PIKA. The analyzed data by Igor are stored as a packed experiment (*.pxp) file with the processed data in the form of *.itx. The file in .h5 format is imported into the software for the analysis. First the m/z calibration is done for the selected run followed by the baseline correction of the peak. This is followed by pre-processing the data. After pre-processing, peak shape corrections are done to get a gaussian fit. This process is unit mass resolution (UMR) analysis and prepares raw spectra for HR analysis. UMR processing is followed by high resolution (HR) fit. For HR fitting the peak shape is corrected again to get HR gaussian fit. This process is called HR fit preparation. After this, the HR fit for a selected run number is done by selecting the appropriate ions for each m/z value, generally up to m/z 200. This is followed by HR-MS calculation.

The IGOR software has two inbuilt checkpoints to identify any deviation within any of the runs during the experiment. First check happens while correcting the baseline of the peak in UMR data processing. The second check happens during the correction step which is done after pre-process in UMR. If the software gives a negative value during the correction step, then the corresponding run number for that point can be found and blacklisted from the data analysis. IGOR also helps to identify if background ions like N2 and CO at m/z 28 and m/z 44 respectively are selected during the ion selection while carrying out the HR fit of the mass spectra. These internal checks by the data analysis software help to review, verify and validate the data obtained from the experiment. To further verify and validate the data collected from the AMS, the results were cross compared with the data acquired using SMPS.

After the data was analyzed in the Igor software, time series for total organic concentration, Chlorine, NH4, NO3, and SO4 were obtained and plotted as seen in section 4.2.

SEMS, CO, GPS, RH, and Temperature:

Aerosol particle size distribution data from the SEMS were generated by the default program from Brechtel, Inc. The data was saved as the native *.csv file. Data from the CO monitor was saved in the form of a *.dat file and averaged every minute. GPS data was saved in *.csv format and was averaged every minute. Data from the temperature and relative humidity was saved in the form of *.txt file.

After all the data was processed and averaged every minute, AMS, Vocus, CO, and GPS data were merged based on their timestamps.

2.6 Overview and Setup of the CMAQ model

A modified version of the Community Multiscale Air Quality (CMAQ) model was updated to use the detailed version of the SAPRC-11 photochemical mechanism (SAPRC-11D) to determine the concentrations of volatile chemical products (VCPs) in the Houston area. The SAPRC-11 chemical mechanism is the updated version of the widely used SAPRC-07 chemical mechanism. The SAPRC-11D differs from other versions of the SAPRC mechanism by explicitly representing the oxidation of a large number of precursor VOCs and it was shown to outperform the lumped SAPRC-11L mechanism in predicting O_3 concentrations in the Houston area (AQRP project 12-006). The SAPRC-11D has been used for SOA modeling in the US and China (7, 8).

Our group has recently updated the CMAQ model with SAPRC-11D to improve its representation of SOA formation from monoterpenes (9). In the modified model, emissions of five major monoterpenes (i.e., α-pinene, β-pinene, d-limonene, Δ^3-carene, and sabinene) and their photochemical reactions are tracked individually. SOA yields from these explicit monoterpene species from OH, NO_3, and O_3 oxidations have also been updated. The SAPRC-11D is also suitable for studying oVCPs. The reactions of major oVCPs, including methanol, ethanol, isopropanol, ethylene glycol, propylene glycol, glycerol, and acetone, are explicitly represented by the mechanism, which will lead to a more accurate representation of PAN, and thus O_3 formation in downwind areas.

Four different episodes were modeled, October 16-31, 2022, November 1-12, 2022, and January 12-24, 2023.

Model input parameters:

Biogenic emissions were generated using the Model of Emissions of Gases and Aerosols from Nature (MEGAN) v3.1. The MEGAN model was modified to generate emissions of detailed VOC emissions that match the species in the SAPRC-11D mechanism.

Anthropogenic emissions were generated using the 2019 Emissions Modeling Platform (https://www.epa.gov/air-emissions-modeling/2019-emissions-modeling-platform), which is based on the 2017 National Emission Inventory released in the spring of 2020 with updates to specific sectors to represent emissions from 2019. The technical details of the 2019 Emissions Modeling Platform can be found in the technical support document (https://www.epa.gov/air-emissions-modeling/2019-emissions-modeling-platform-technical-support-document). The Emission Platform provides detailed emission inventory files and auxiliary files needed to process the emission inventory to generate model-ready emissions using the Sparse Matrix Operator Kernel Emissions (SMOKE) model.

Relevant to this project, the evaporative emissions from non-point sources of solvent utilization (np_solvents), including emissions from everyday items, such as cleaners, personal care products, adhesives, architectural and aerosol coating, printing inks, and pesticides, are derived using the volatile chemical products in Python (VCPy) framework, as described by Seltzer et al. (2). In this framework, the emission of an organic compound from a product depends on the magnitude of the product use timescale and the evaporation timescale of the component. Emission occurs if the evaporation timescale is less than the assigned product use timescale. The evaporation timescale is affected by the composition of these products, and the physiochemical properties of their constituents that govern volatilization. National-level emissions, estimated using economic statistics data from the U.S. Census Bureau, are allocated to county-level using proxies, such as population, employment statistics, and pesticide use. Point source solvent emissions are removed from the np_solvents sector to avoid double counting.

Speciation of the VOC emissions was based on the speciation profiles used in the 2019 Emissions Modeling Platform. To generate speciation profiles suitable for the SAPRC-11D mechanism, all VOC profiles in the US EPA's SPECIATE profiles database were downloaded and processed using the SpecDB program (https://intra.engr.ucr.edu/~carter/emitdb/) from Dr. William Carter of UC Riverside.

Spatial and temporal distributions of VCPs is modeled using nested domains with 36, 12, 4, and 1.33 km spatial resolutions. The 36, 12, and 4-km domains will match those used by the Texas

Commission on Environmental Quality (TCEQ) for the 8-h O_3 modeling (https://www.tceq.texas.gov/airquality/airmod/data/domain). Within the 4-km resolution domain, the finer resolution (1.33-km) domain is nested to provide the detailed spatial distribution of air pollutants in the Greater Houston area. The spatial allocation surrogates at different model resolutions were generated using the shapefiles included with the 2019 Emissions Modeling Platform and the Spatial Allocator program (https://www.cmascenter.org/sa-tools/). Figure 1 shows the average emissions of n-hexane and d-Limone in the 1.33-km Houston domain for the November 2022 modeling episode.

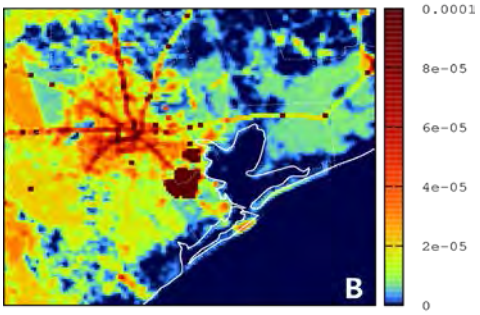

Figure 2.6.1. 2022 November modeling episode average emissions of n-hexane (A) and d-limonene (B) in the 1.33-km Houston domain.

Meteorology inputs to the CMAQ model were generated using the Weather Research and Forecasting (WRF) model v4.4. The WRF simulation used 44 vertical layers, which is the same as the one used by the TCEQ in the 2021 Regional Haze State Implementation Plan (SIP) modeling. The European Centre for Medium-Range Weather Forecasts (ECMWF) Reanalysis v5 (ERA5), the fifth generation ECMWF of the global climate, which provides hourly reanalysis meteorological fields at 137 model levels with a resolution of 0.25x0.25 degrees, were used as model inputs to drive the WRF model. The performance of the model was evaluated against surface observation data collected by the National Center for Environmental Prediction (NCEP) (dataset ds461.0). The overall model performance based on all the stations is shown in Table 1.

Table 2.6.1. Model performance statistics for surface temperature (T), wind speed (WS), wind direction (WD) and relative humidity (RH) at all monitors in the 1.33-km domain

Variable	MB	GE	RMSE	Obs.	Pred.
T (K)	-0.33	1.72	2.13	284.54	284.21
WD (°)	12.42	26.26	39.56	184.09	167.42
WS (m/s)	0.18	1.18	1.53	3.73	3.91
RH (%)	1.16	9.15	11.8	74.05	72.9

2.7 Model performance evaluation

Criteria pollutants:

The concentrations of PM2.5, NO2, and O3 at monitoring sites are provided by TCEQ. Figure 2.7.1 shows the locations of the PM2.5 monitoring stations in the 1.33-km resolution model domain. As shown in Figure 2.7.2, the predicted hourly PM2.5 concentrations in November 2022 agree well with the model predictions, although on November 5 and 6 the model seemed to have systematically overpredicted the PM2.5 concentrations at all monitoring sites. Figures 2.7.3-2.7.5 show the locations as well as the predicted and observed NO2 concentrations at three monitoring stations. In total, 21 monitoring stations were analyzed but due to a limit of page, only 3 samples are shown in the figures. Ozone concentrations are generally low in November. The model captured the higher O3 concentrations during the day but often overpredicted the nighttime concentrations, especially at sites that are suburban or rural areas. It is likely that the vertical mixing at these areas were overestimated in the model under nighttime, leading to excess downward mixing of O3 from upper layers.

The results below show that observations at the suburban and rural sites did not shown as much low concentrations at night as those in November, and the model predictions agree with the observations better. The model performance of NO2 in October is similar to that of November. The time series plots are included below.

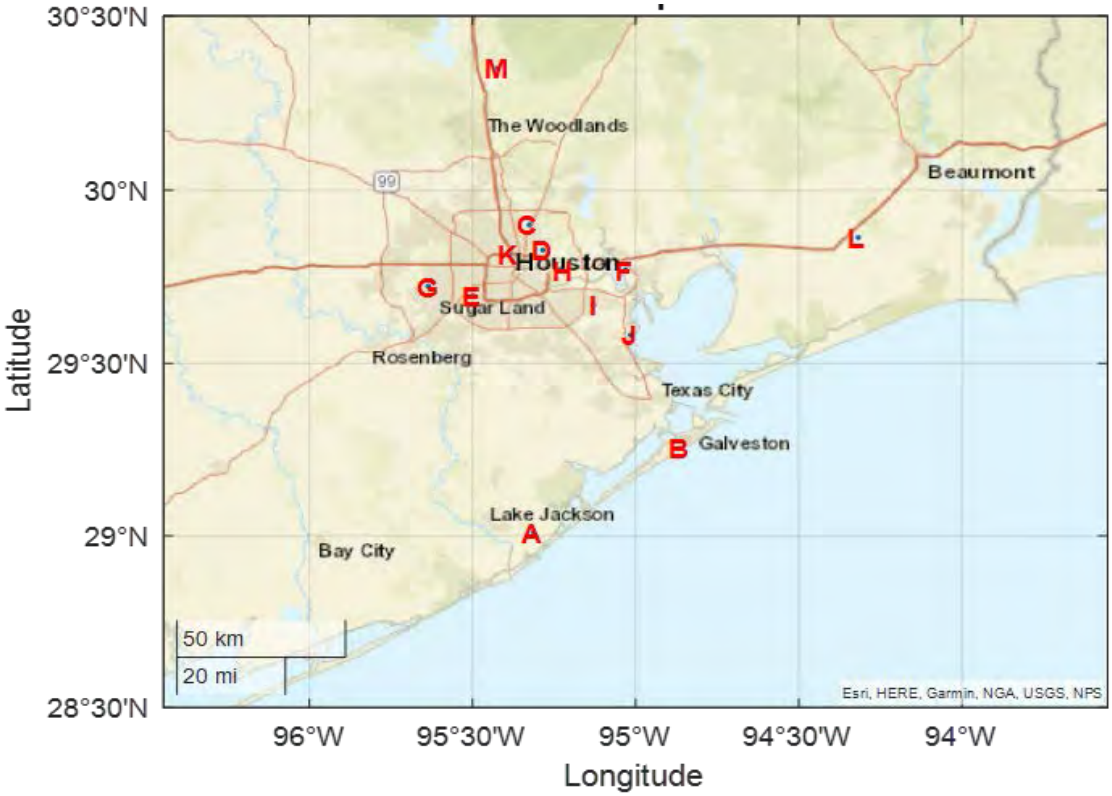

Figure 2.7.1. The location of the PM2.5 monitoring sites.

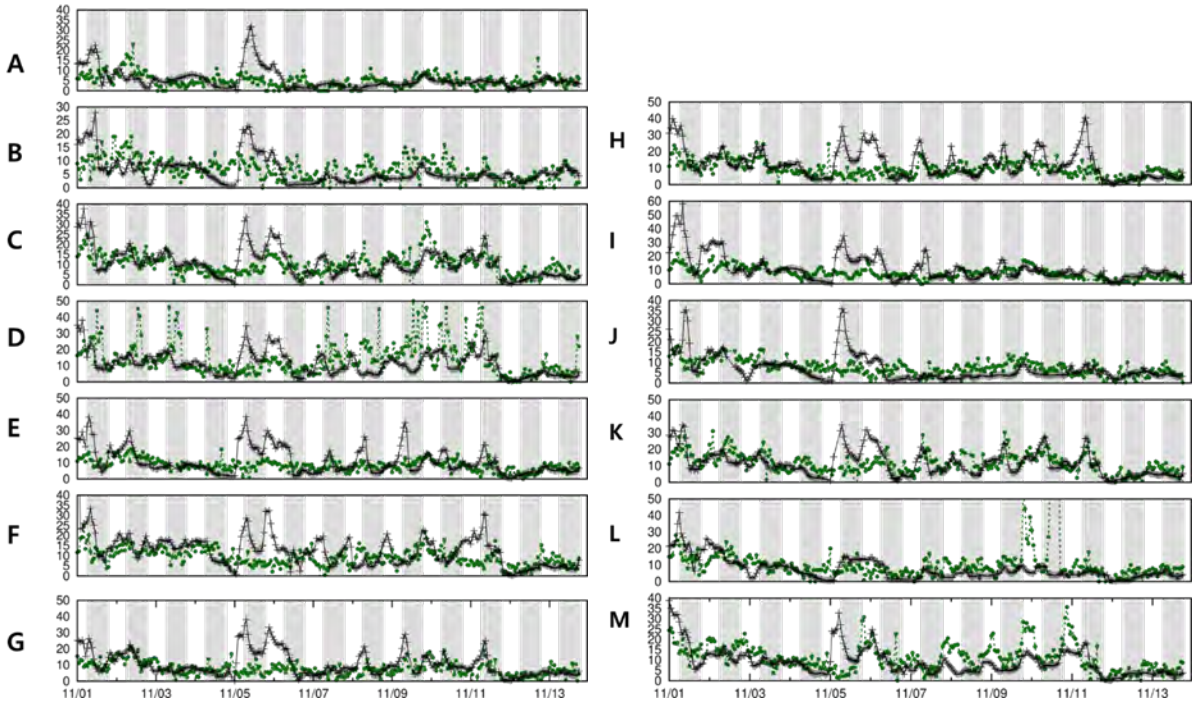

Figure 2.7.2. Predicted (black) and observed (green) PM2.5 concentrations at monitor sites for November 1 to November 15, 2022. The shaded areas represent daytime hours (7 am to 6 pm). The monitor sites are 480391607 (A), 481671034 (B), 482010024 (C), 482010046 (D), 482010055 (E), 482010058 (F), 482010066 (G), 482011034 (H), 482011039 (I), 482011050 (J), 482011052 (K), 482450022 (L), and 483390078 (M).

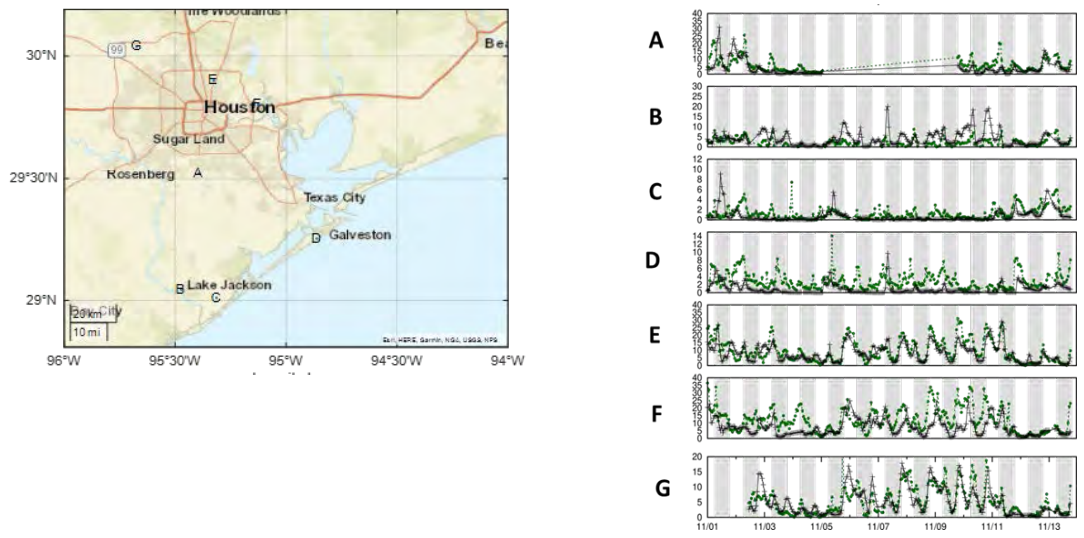

Figure 2.7.3. Location of the NO_2 monitoring sites (left) and predicted (black) and observed (green) NO2 concentrations for November 1 to November 15, 2022. The shaded areas represent daytime hours (7 am to 6 pm). The monitor sites are 480391004 (A), 480391016 (B), 480391607 (C), 481671034 (D), 482010024 (E), 482010026 (F), and 482010029 (G).

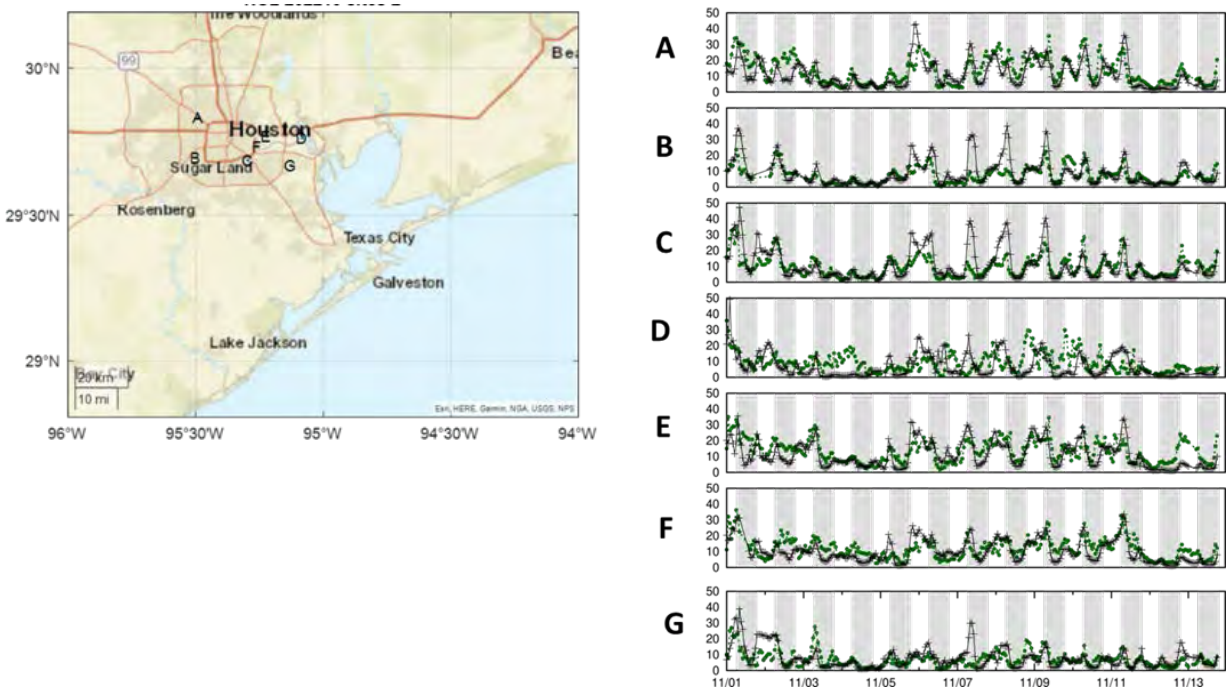

Figure 2.7.4. Location of the NO_2 monitoring sites (left) and predicted (black) and observed (green) NO2 concentrations for November 1 to November 15, 2022. The shaded areas represent daytime hours (7 am to 6 pm). The monitors are 482010047 (A), 482010055 (B), 482010416 (C), 482011015 (D), 482011034 (E), 482011035 (F), and 482011039 (G).

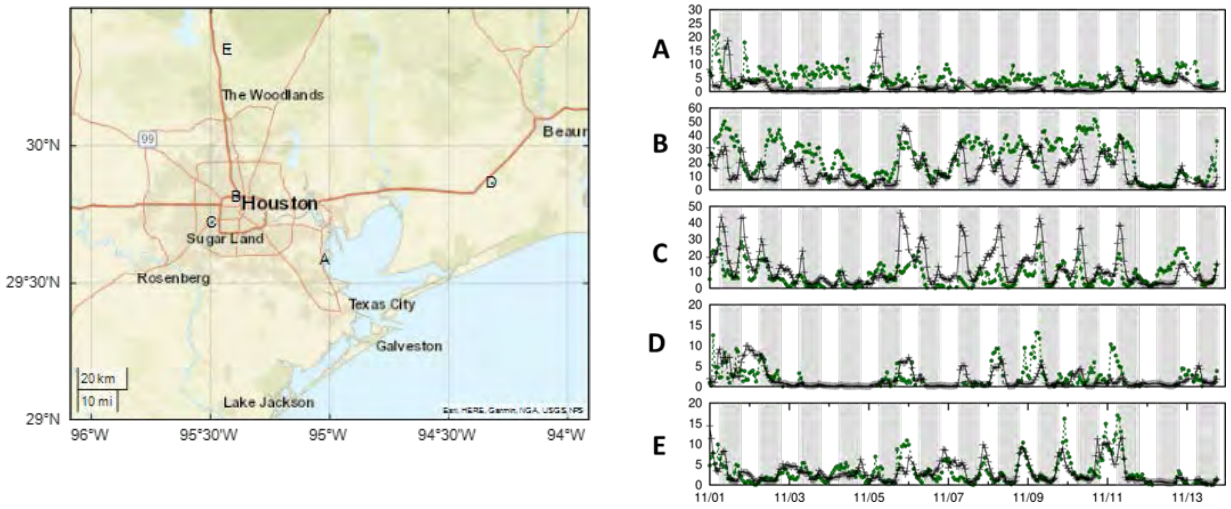

Figure 2.7.5. Location of the NO_2 monitoring sites (left) and predicted (black) and observed (green) NO2 concentrations for November 1 to November 15, 2022. The shaded areas represent daytime hours (7 am to 6 pm). The monitors are 482011050 (A), 482011052 (B), 482011066 (C), 482450022 (D), and 483390078 (E).

Cross comparison of organic compounds at the AutoGC sites:

In addition to the criteria pollutants, the modeled VOC concentrations were compared with the hourly concentrations measured by the Automated Gas Chromatographs (AutoGC) at 5 monitor sites (Figures 2.7.6-2.7.11). The predicted and observed concentrations of selected VOC species in November 2022, including propane (C3H8), n-pentane (C5H12), n-hexane (C6H14), n-heptane (C7H16), n-octane (C8H18), n-nonane (C9H20), n-decane (C10H22), toluene, o-xylene, and acetylene, are shown in Figures 13-22, respectively. The model did a better predicting the concentrations of larger alkanes (C6-C10) than the smaller ones (C3-C5). As the smaller alkanes are likely to have larger contributions from VCPs (2), it is likely that VCP emissions of these species were underestimated. The aromatic compounds, represented by toluene and xylenes, and are mainly from combustion sources, were predicted reasonably well.

Figure 2.7.6. The locations of the auto-GC monitoring sites 482010069 (A), 482010307 (B), 482010803 (C), 482011035 (D), and 482016000 (E).

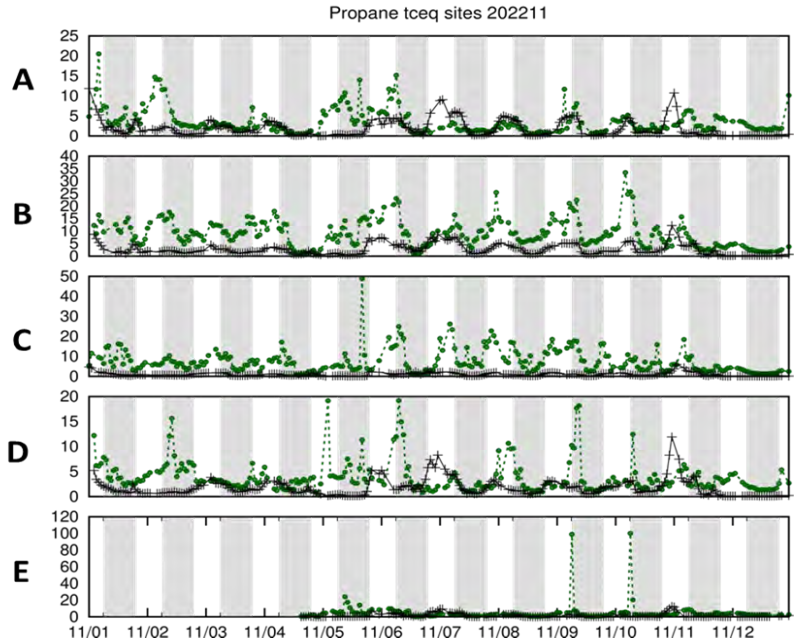

Figure 2.7.7. Predicted (black) and observed (green) propane concentrations for November 1 to November 15, 2022. The shaded areas represent daytime hours (7 am to 6 pm).

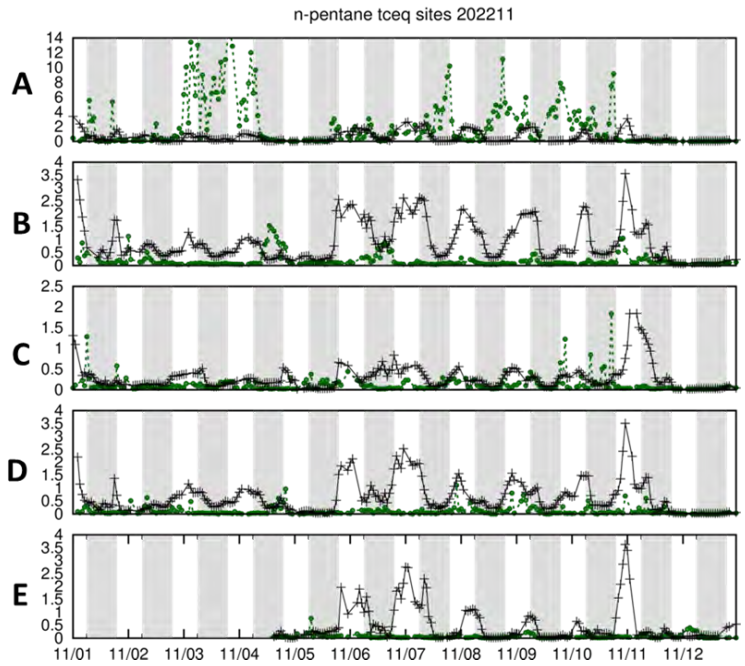

Figure 2.7.8. Predicted (black) and observed (green) n-pentane concentrations for November 1 to November 15, 2022. The shaded areas represent daytime hours (7 am to 6 pm).

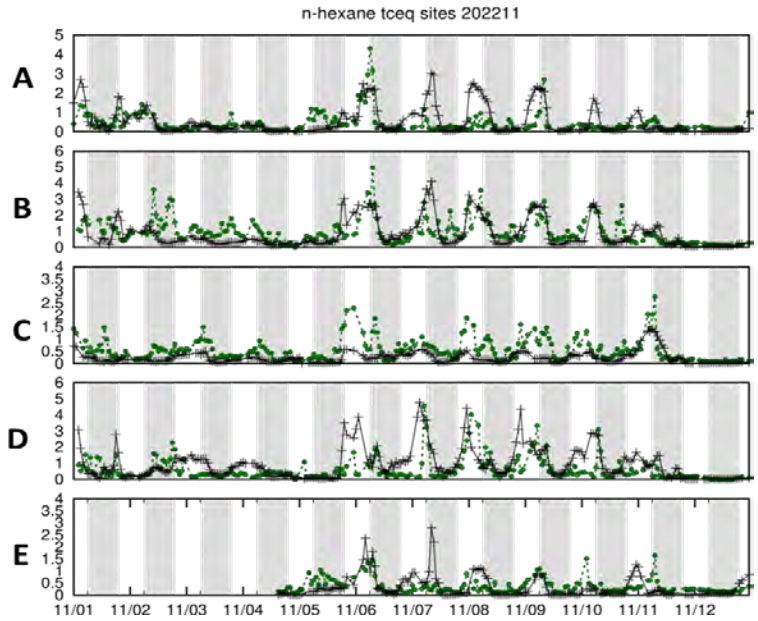

Figure 2.7.9. Predicted (black) and observed (green) n-hexane concentrations for November 1 to November 15, 2022. The shaded areas represent daytime hours (7 am to 6 pm).

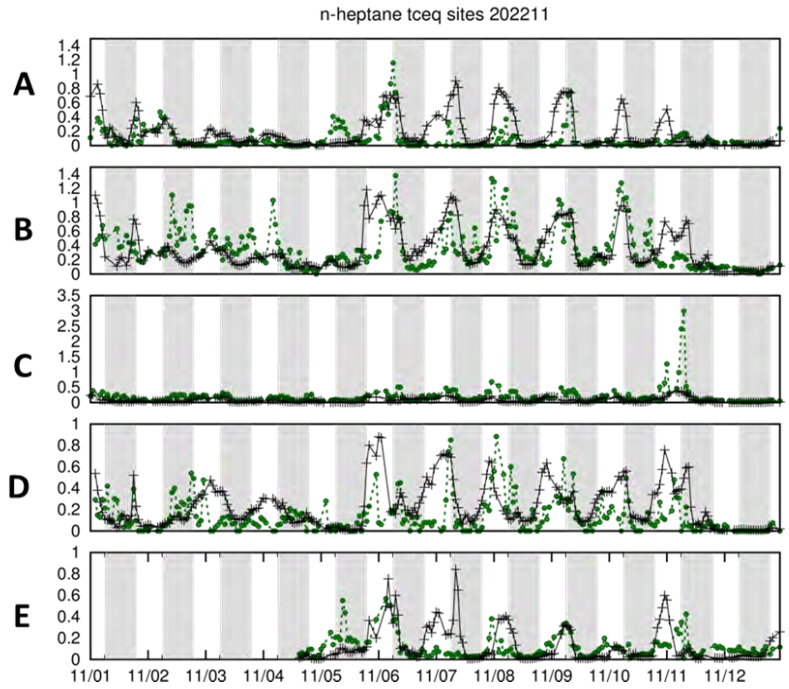

Figure 2.7.10. Predicted (black) and observed (green) n-heptane concentrations for November 1 to November 15, 2022. The shaded areas represent daytime hours (7 am to 6 pm).

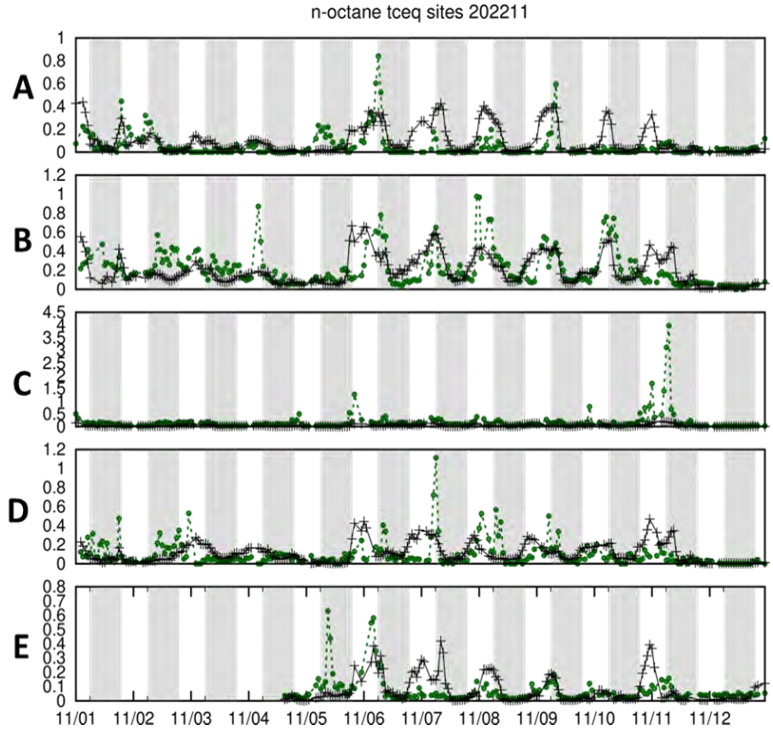

Figure 2.7.11. Predicted (black) and observed (green) n-octane concentrations for November 1 to November 15, 2022. The shaded areas represent daytime hours (7 am to 6 pm).

3. Quality Assurance and Quality Check

3.1 QA/QC for Analytical Instruments

SP-HR-ToF-AMS: The quality control of AMS data was performed the following steps. Firstly, before the operation, calibration procedures were performed. The detailed calibration methods are described in section B7. Briefly, ionization efficiency (IE) calibration was performed at an interval of two weeks. Flow rate calibration was performed along with the IE calibration every two weeks. Particle time of calibration was performed if the instrument at the beginning of the campaign. Secondly, during the operation, *m/z*calibration was performed once daily before starting the analysis. Thirdly, after the experiments, the data were imported into the PIKA Igor analysis software, where the flow rate and all voltages of the instrument during the operational period were examined. We removed bad data points based on these benchmark values and remove them from the analysis software.

HR-ToF-Vocus CIMS Instruments: The quality control of Vocus CIMS data was performed the following steps. Firstly, before the sampling, the calibration procedures were performed weekly under laboratory conditions. Secondly, prior to daily sampling, while the Vocus was sampling ambient air, the obtained mass spectrum should have specific ions as the highest. Under the PTR mode, the highest ions were *m/z* 55 ($(H_2O)_2H_3O^+$), *m/z* 59 ($C_3H_7O^+$), *m/z* 37 ($(H_2O)H_3O^+$), and *m/z* 73 ($(H_2O)_3H_3O^+$). With NH_4^+ mode, the highest ions weree *m/z* 76 ($(C_3H_6O)NH_4^+$), *m/z* 36 ($(H_2O)NH_4^+$), *m/z* 35 ($(NH_3)NH_4^+$), and *m/z* 54 ($(H_2O)_2NH_4^+$). Thirdly, after the experiments, the data analysis of Vocus were performed using the Tofware package (version 3.2.3) running in the Igor Pro. The status of the instrument was examined during the data processing, and any bad data points based on the benchmark values were removed from the data set.

Other Instruments: The aethalometer, NO_2 analyzer, and CO analyzer provided black carbon, NO_2, and CO concentrations. Filter sampler was analyzed by a high-resolution mass spectrometer to identify the chemical composition of aerosols. These instruments were provided in-kind by other unfunded collaborators and their usage was dependent on availability during the campaign period.

3.2 QA/QC for Models

Dr. Ying has beenresponsible for all QA activities related with air quality modeling, including an audit of the data quality for the model input data and those data produced by the models. The Civil and Environmental Engineering (CVEN) graduate student Hee Won performed most of the actual model simulation and generate all the data. A minimum of 10% of the input and output data have been audited by Dr. Ying. Dr. Ying and the CVEN student will cross-examine any additional source code developed to ensure all coding errors are fixed before using the model for production runs.

The input data to run Weather Research and Forecasting (WRF0 (i.e., the final (FNL) global analysis) have been quality assured thus no additional QA is needed for them. Selected run scripts (at least 10%) prepared by the student were examined by Dr. Ying during the QA step. Afterwards, WRF outputs will be compared with observations (acquired from the National Climate Data Center) as part of the QA process. In addition to overall model performance statistics, timeseries of predictions at stations in southeast Texas were examined to detect any irregular model results. Input data and run scripts were double checked for these periods identified.

The input data to generate the biogenic and anthropogenic emissions (i.e., land use/land cover data, the national emission inventories, and the FINN fire inventory) all have been quality assured in

the institutions that developed them, thus no additional QA is needed. Run scripts generated by the student (10% minimum) were checked by Dr. Ying. Calculated emissions will be plotted (at least 10% of the data), both in the form of regional distributions and time series and examined manually by Dr. Ying to ensure the quality of the data.

4. Results

The results of the data are shown below in the following plots. We organize the results with VCP data, AMS data, and seasonal difference.

4.1 VCP Data

There are altogether 61 VCPs that we have quantified, of which we select a few key species including texanol, parachlorobenzotrifluoride (PCBTF), monoterpenes, acetone, D5-siloxane, and methylethylketone (MEK). We thoroughly analyzed all the field data of these species to identify their season variation as well as their ozone formation potential.

Due to the natural of mobile lab deployment where there will be emission from other vehicles that can also enhance VCP emissions, we decide to both analyze the VCP concentration and the VCP:CO for each day. The ratio of VCP:CO can characterize for the VCP contribution from other sources versus combustion as CO is often regarded a tracer for combustion. In total we analyzed and plotted more than 126 graphs. Due to the limit of page, we show a few examples of graphs and summarize the results below.

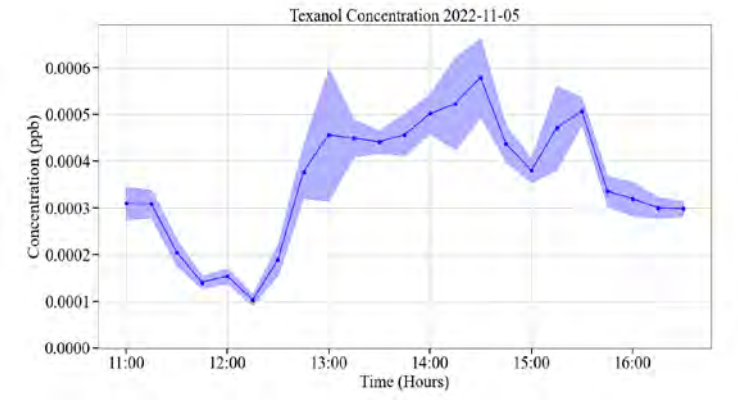

Figure 4.1.1a – Sample Texanol Concentration in Fall 2022

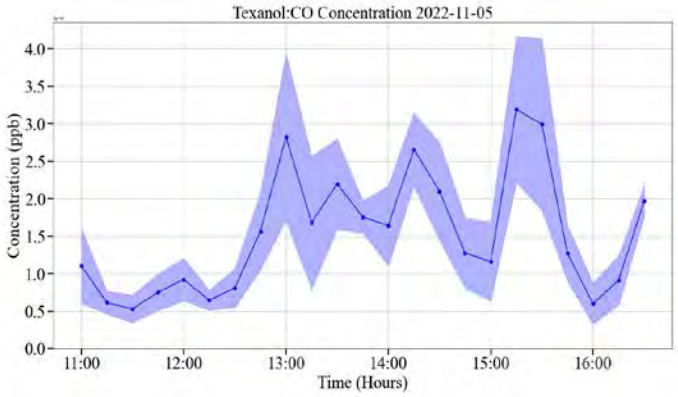

Figure 4.1.1b - Sample Texanol:CO Ratio in Fall 2022

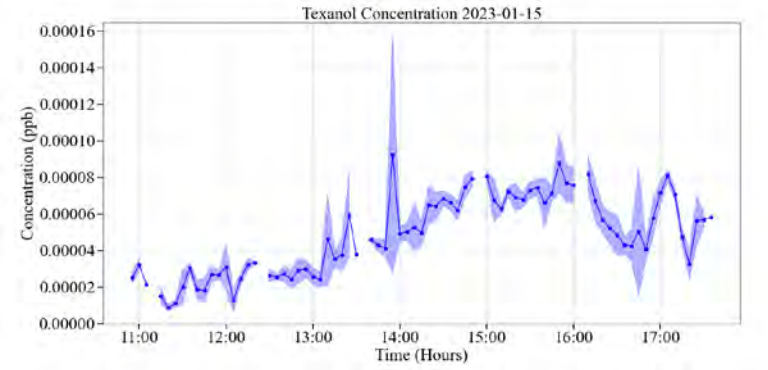

Figure 4.1.2a - Sample Texanol Concentration in Winter 2023

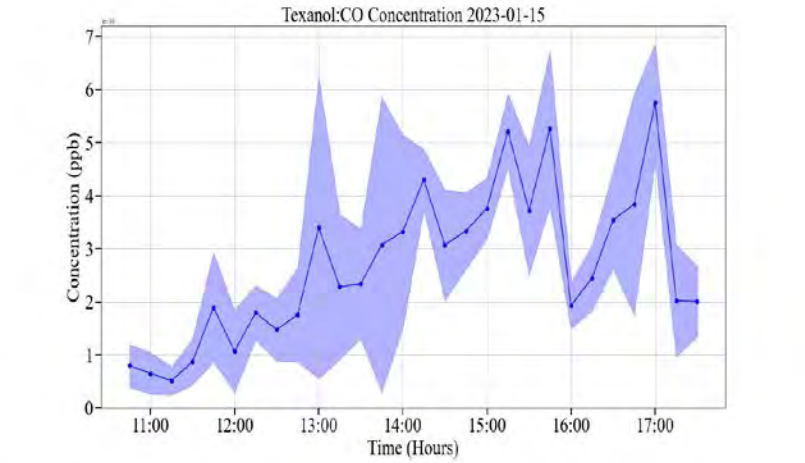

Figure 4.1.2b - Sample Texanol:CO Ratio in Winter 2023

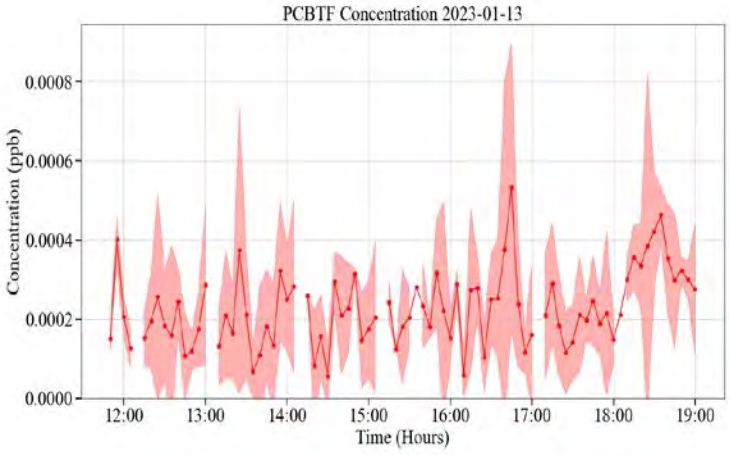

Figure 4.1.3a - Sample PCBTF Concentration in Fall 2022

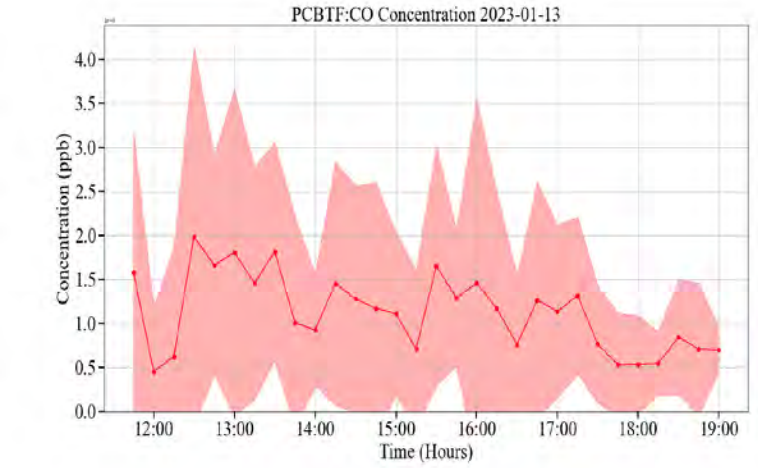

Figure 4.1.3b - Sample PCBTF Concentration in Winter 2023

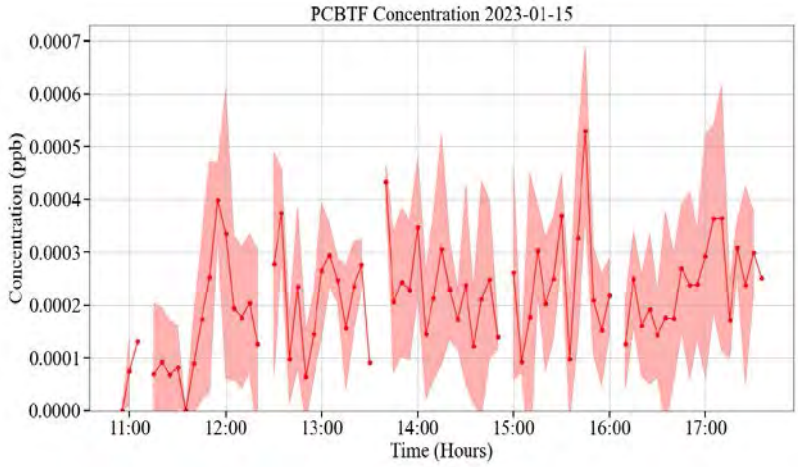

Figure 4.1.4a - PCBTF Concentration Panel K

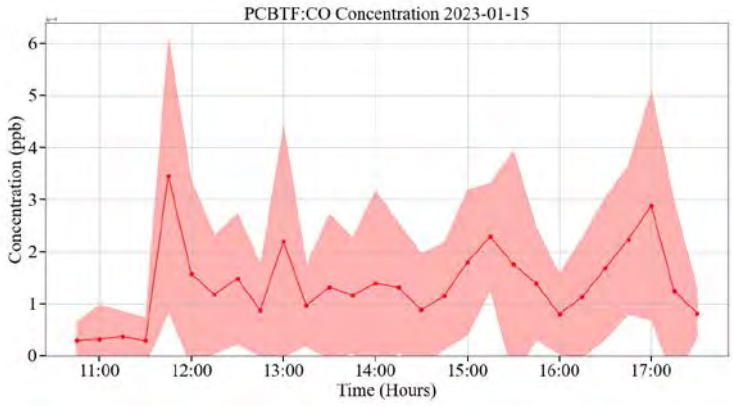

Figure 4.1.4b - Sample PCBTF:CO Ratio in Winter 2023

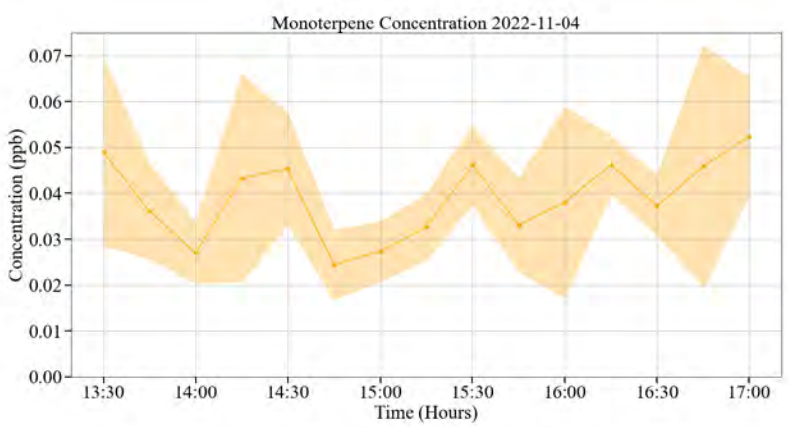

Figure 4.1.5a - Sample Monoterpene Concentration in Fall 2022

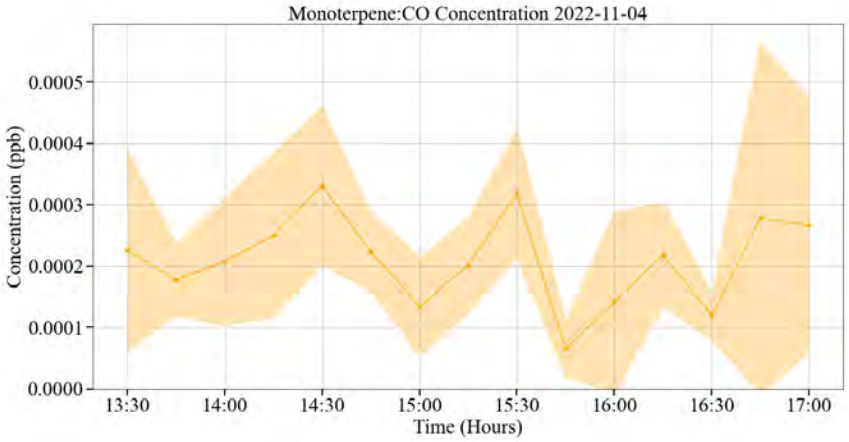

Figure 4.1.5b - Sample Monoterpene:CO Ratio in Fall 2022

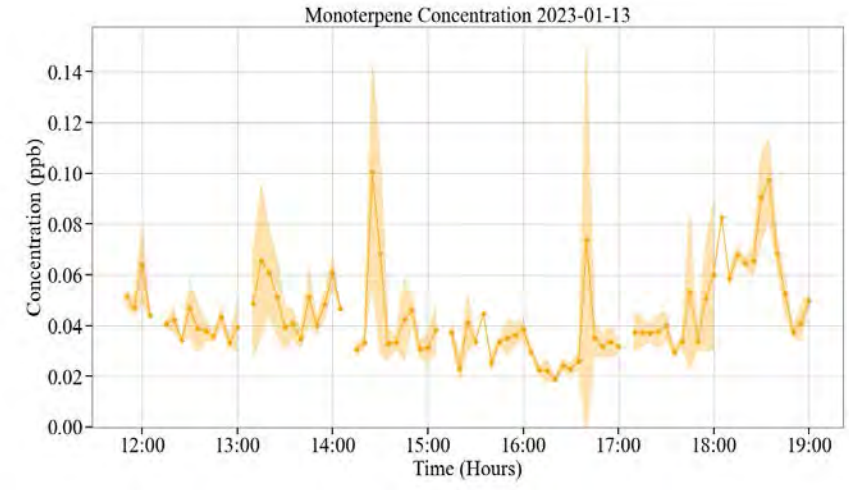

Figure 4.1.6a - Sample Monoterpene Concentration in Winter 2023

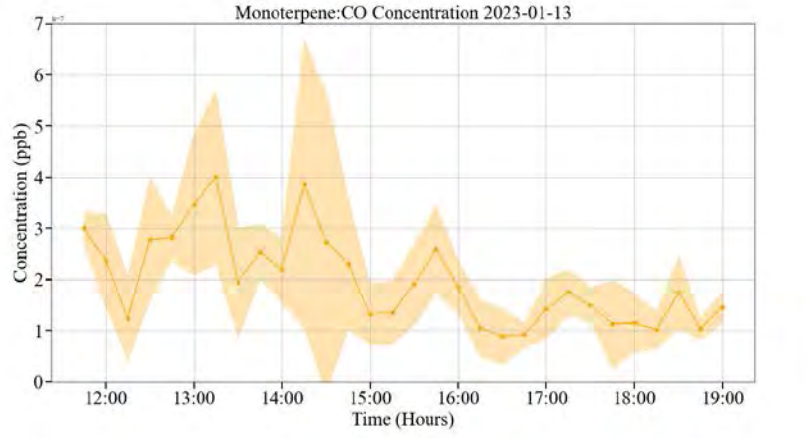

Figure 4.1.6b - Sample Monoterpene:CO Ratio in Winter 2023

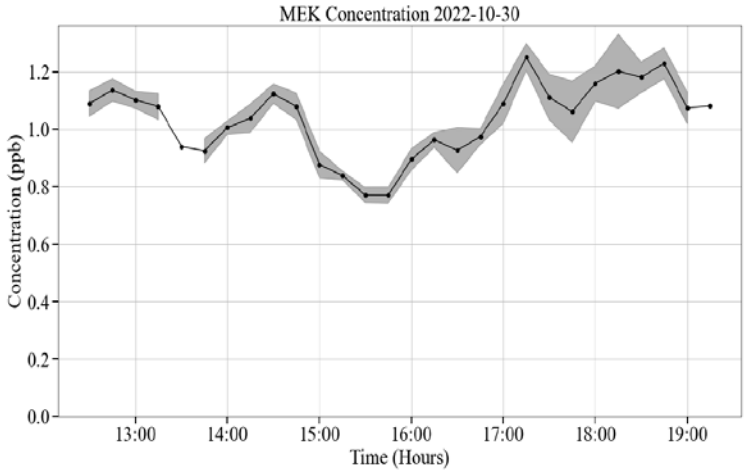

Figure 4.1.7a - Sample MEK Concentration in Fall 2022

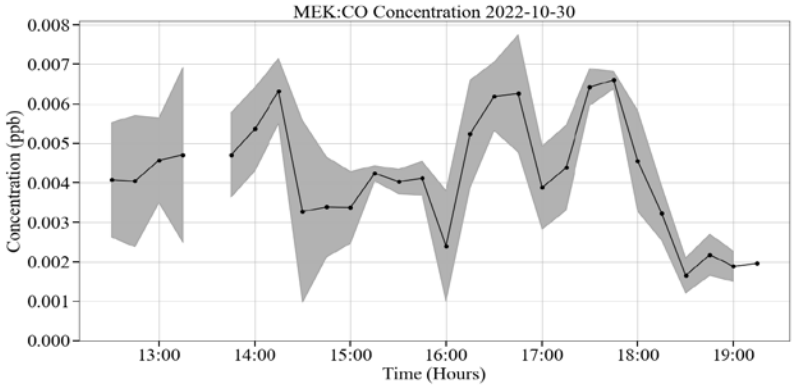

Figure 4.1.7b - Sample MEK:CO Ratio in Fall 2022

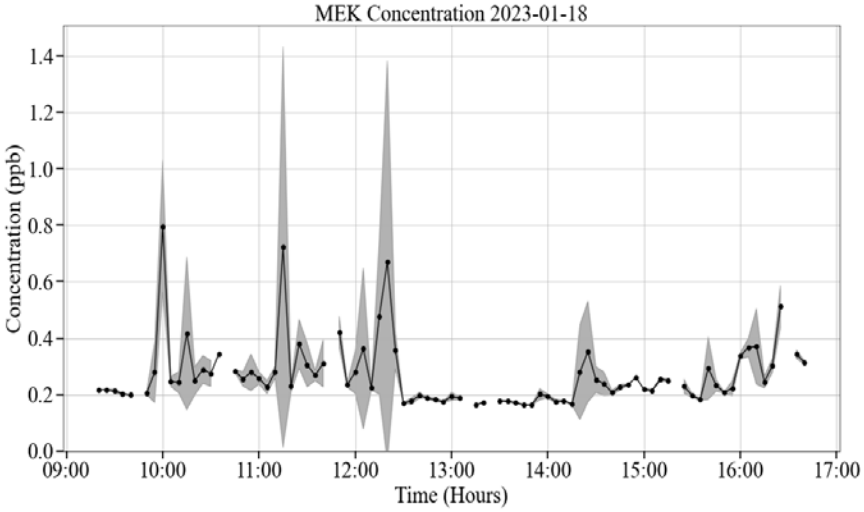

Figure 4.1.8a - Sample MEK Concentration in Winter 2023

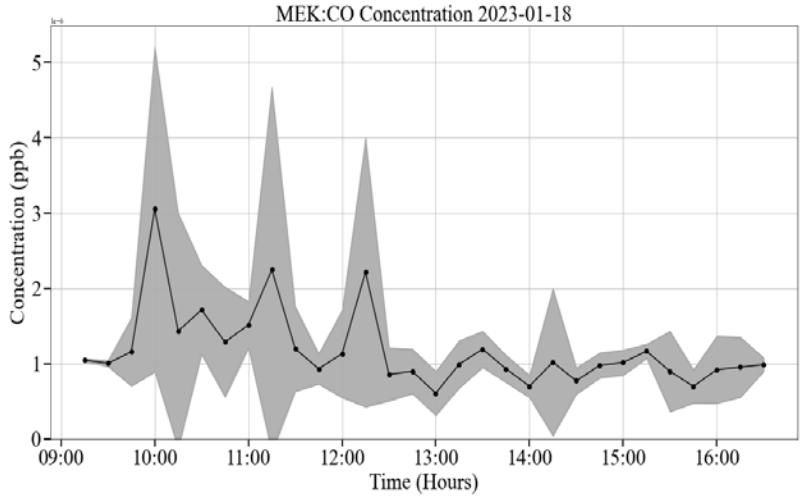

Figure 4.1.8b - Sample MEK:CO Ratio in Winter 2023

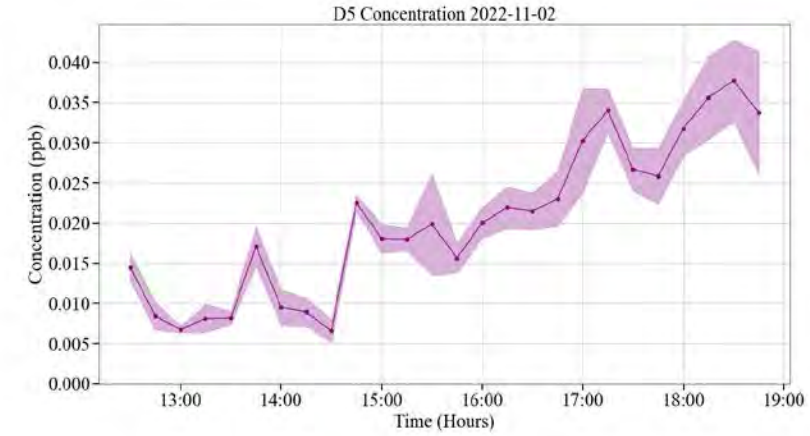

Figure 4.1.9a - Sample D5-Siloxane Concentration in Fall 2022

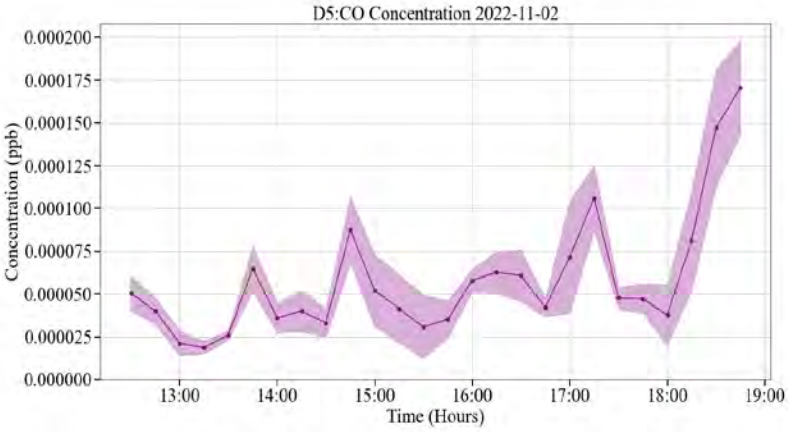

Figure 4.1.9b - Sample D5-Siloxane:CO Ratio in Fall 2022

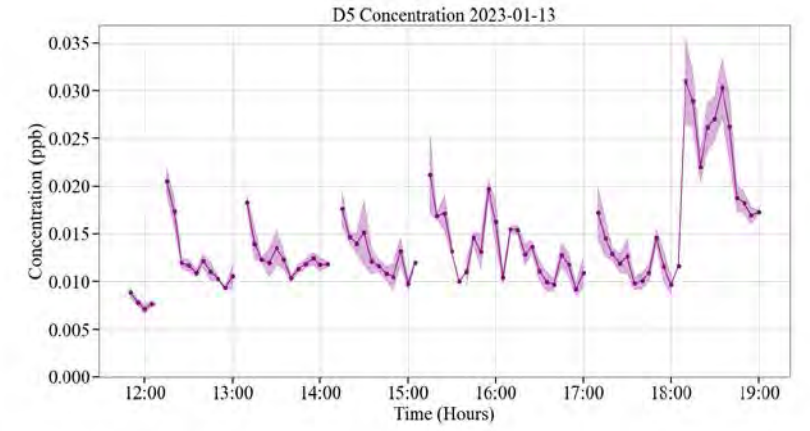

Figure 4.1.10a - Sample D5-Siloxane Concentration in Winter 2023

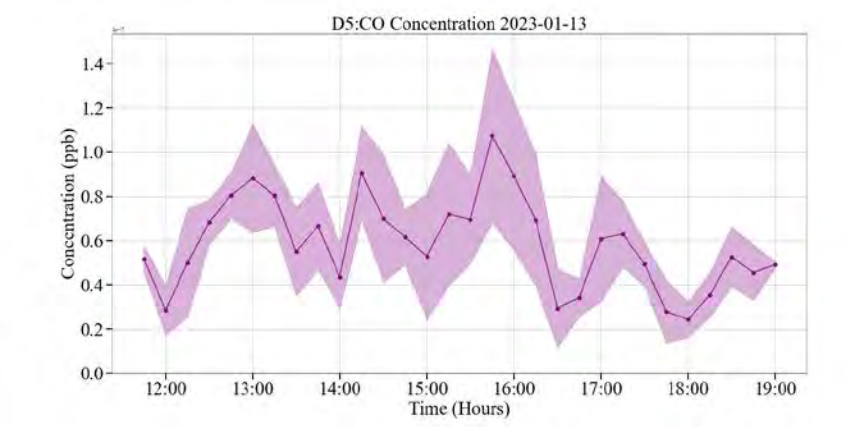

Figure 4.1.10b - Sample D5-Siloxane:CO Ratio in Spring 2023

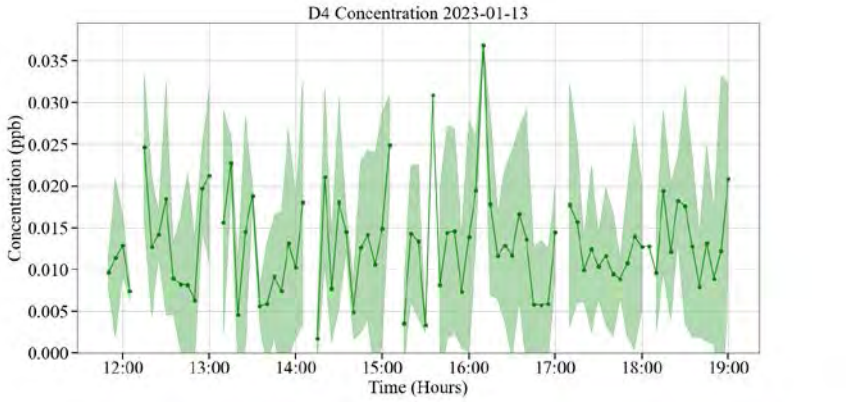

Figure 4.1.11a - Sample D4-Siloxane Concentration in Fall 2022

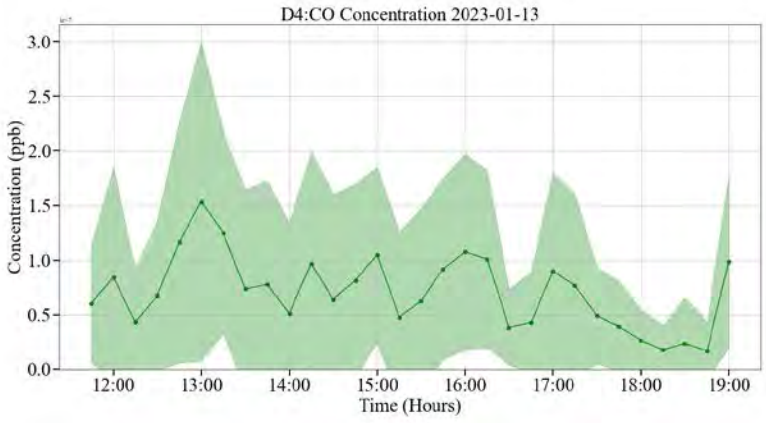

Figure 4.1.11b - Sample Sample D4-Siloxane Concentration in Winter 2023

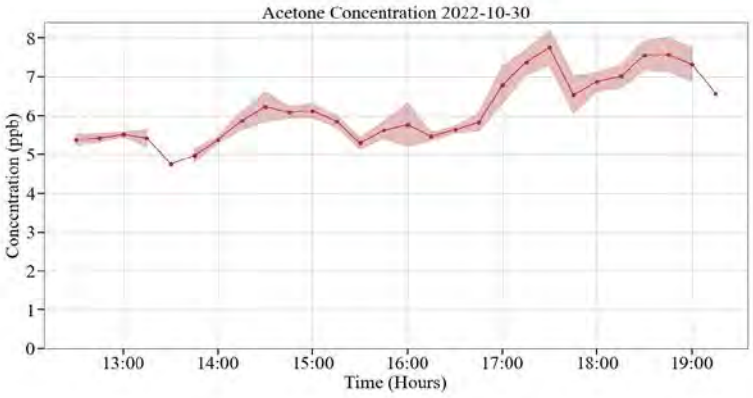

Figure 4.1.12a - Sample Acetone Concentration in Fall 2022

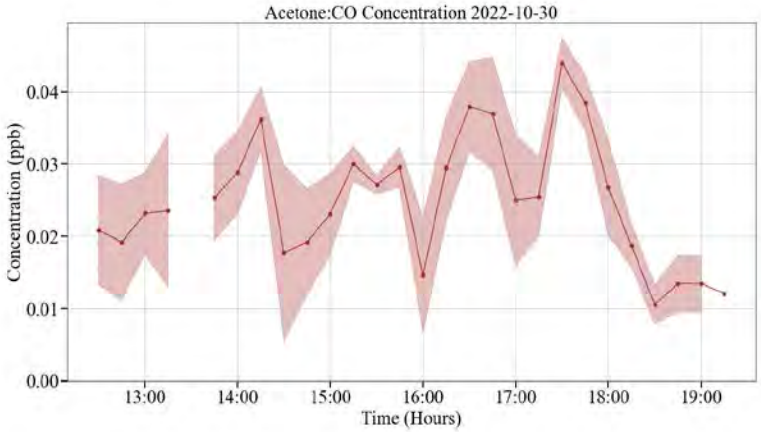

Figure 4.1.12b - Sample Acetone:CO Ratio in Fall 2022

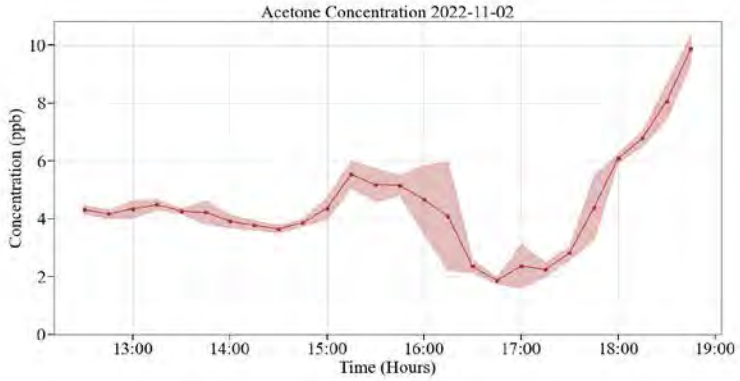

Figure 4.1.13a - Sample Acetone Concentration in Winter 2023

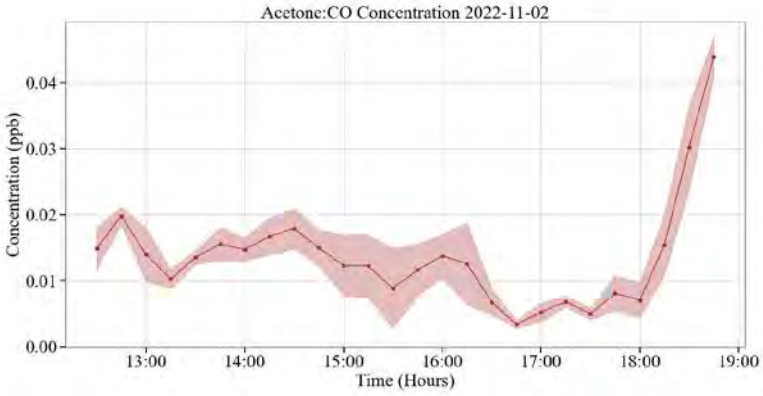

Figure 4.1.13b - Sample Acetone:CO Ratio in Winter 2023

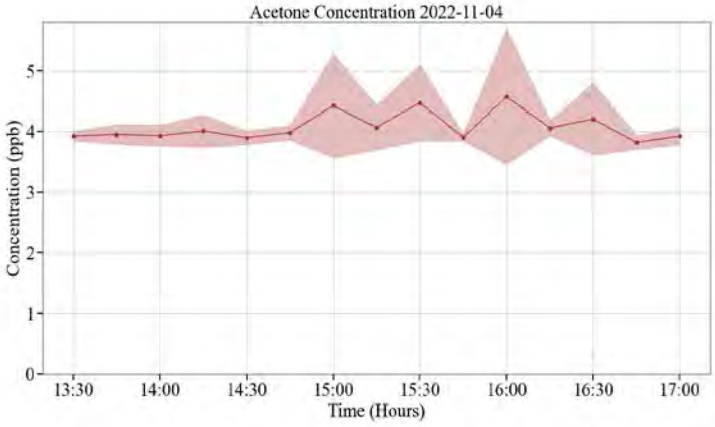

Figure 4.1.14a - Acetone Concentration Panel C

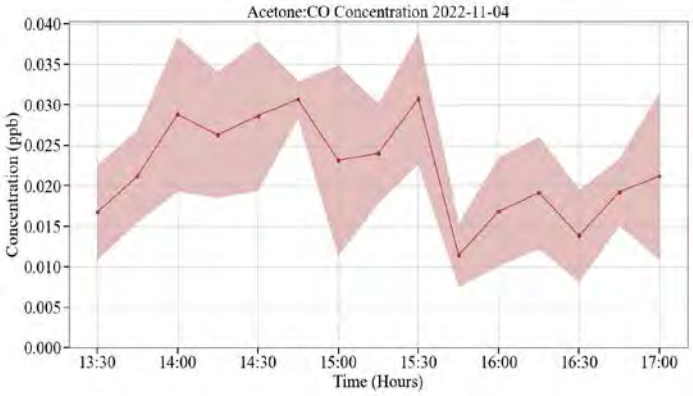

Figure 4.1.14b - Acetone Concentration Panel C

To understand the impact on traffic related VOC emissions on our measurements, and to identify days with stagnant air masses, we analyzed the correlation between VCPs and CO as shown below. Correlation coefficients were calculated to compare each VCP species listed in this report (acetone, MEK, D4-siloxane, D5-siloxane, monoterpenes, PCBTF, and texanol. Correlation coefficients were calculated for the entire day, along with in the morning during rush hour from 9:00-11:00, in

the afternoon from 11:00-16:00, in the evening during rush hour from 16:00-18:00, and in the late evening from 18:00-21:00. We have analyzed all fall and winter data and have made more than 30 plots. Below are the two examples shown in the fall and winter.

It is not evident that there is a strong correlation between any VCP measurements and CO during these time periods. The overall correlation coefficients were always less than 0.3 and often much smaller, even though the data points show that certain times there can be strong correlation. This non-uniform correlation suggests that CO can impact VCPs at certain times, while other times CO may not have a strong influence in the VCPs. The detailed impacts of CO on VCPs need to be further examined.

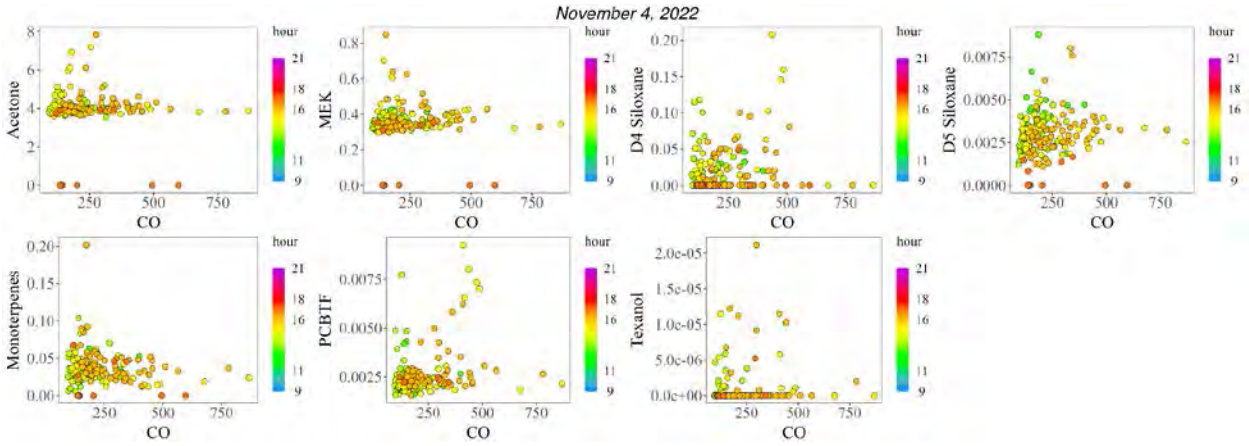

Figure 4.1.15 - November 4, 2022 VCP vs CO concentrations (ppb)

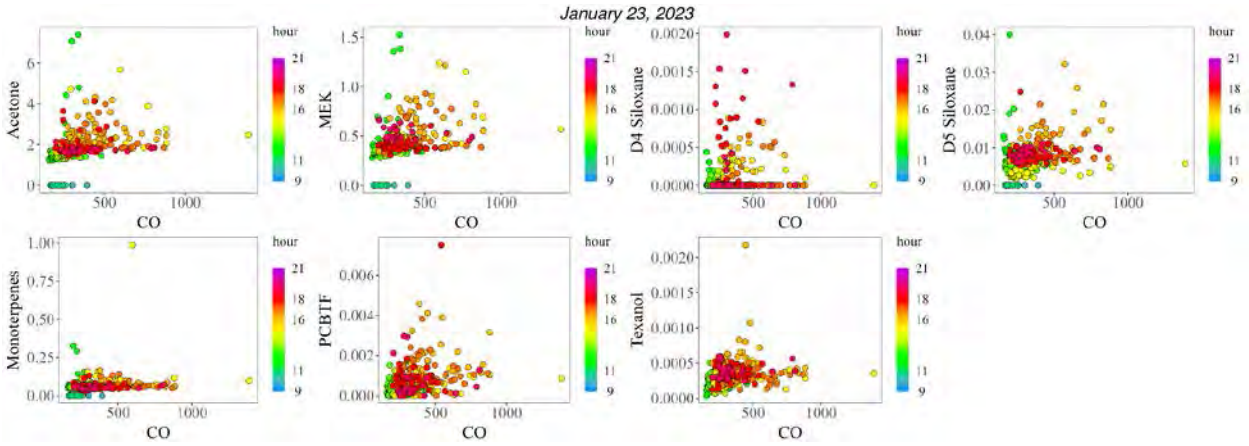

Figure 4.1.16 - January 23, 2023 VCP vs CO concentrations (ppb)

4.2 AMS Data

The AMS data were quality checked, analyzed, and plotted below. Each figure below represents the concentrations of different aerosol species during each day of the field study. Organic aerosols were plotted first, followed by inorganic species. We have plotted more than 60 plots for all data

collected during the fall and winter. Below are two examples of the plots for the winter and the fall.

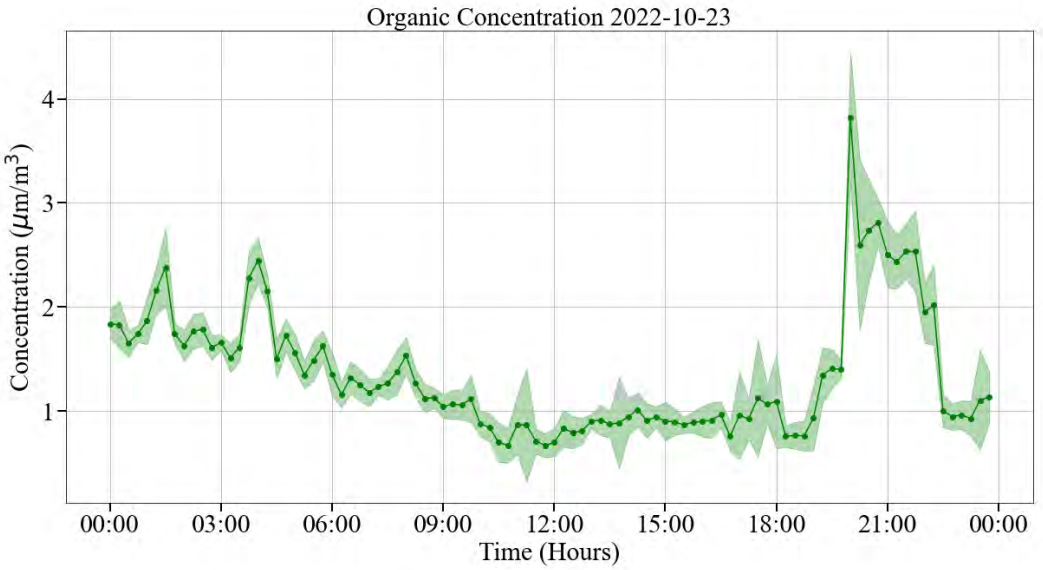

Figure 4.2.1 - Organic Concentration (µg/m^3) October 23, 2022

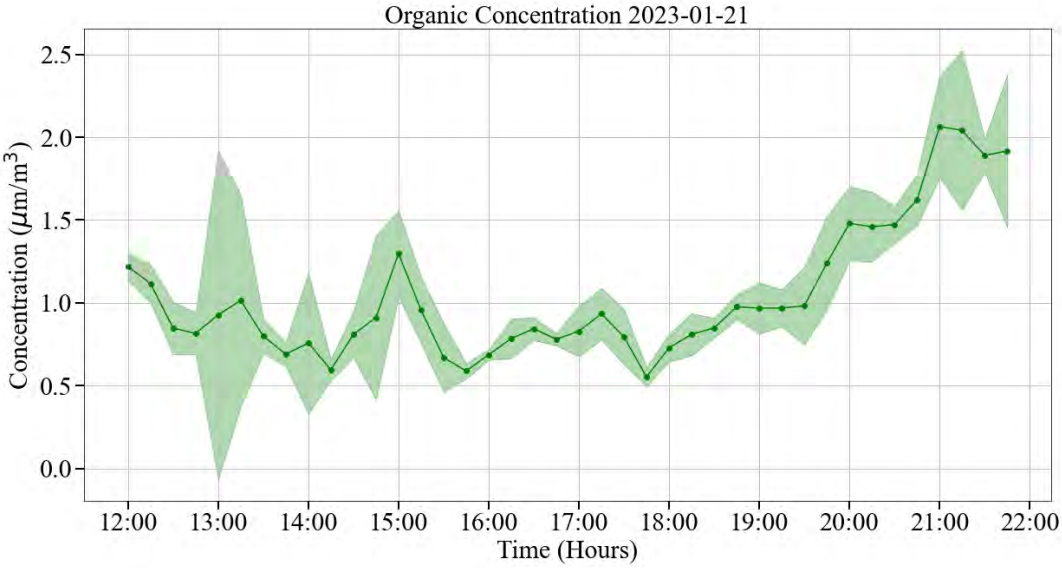

Figure 4.2.2 - Organic Concentration (µg/m^3) January 21, 2023

Inorganic concentrations for each day were shown below.

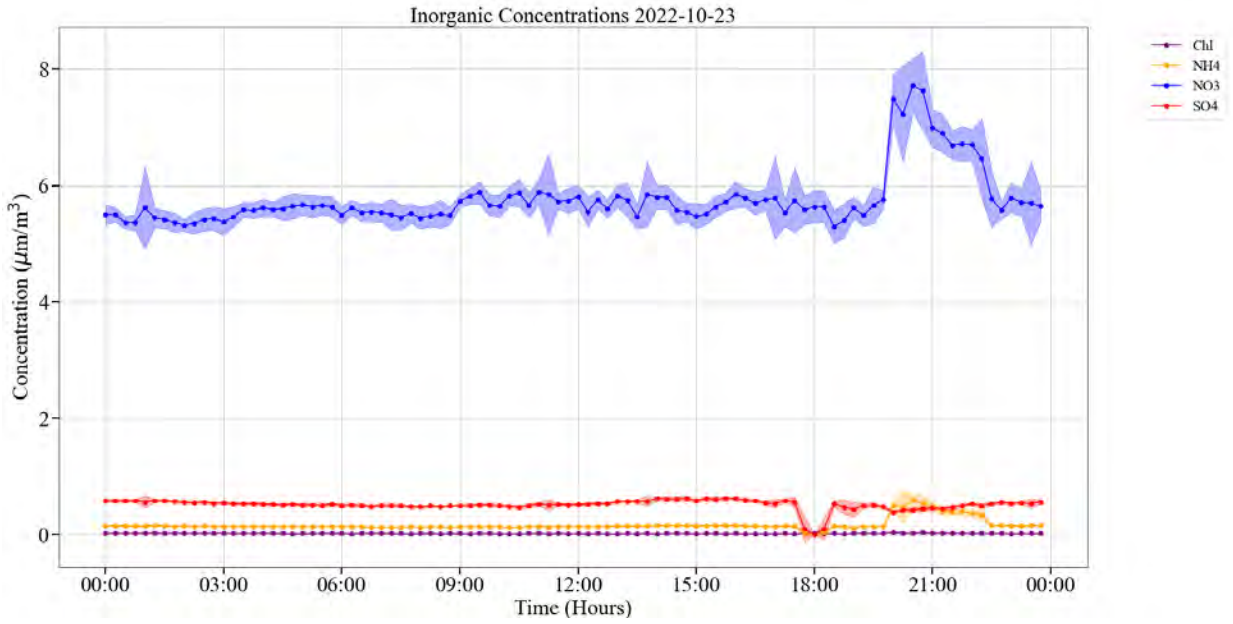

Figure 4.2.3 - Organic Concentration (µg/m^3) October 23, 2022

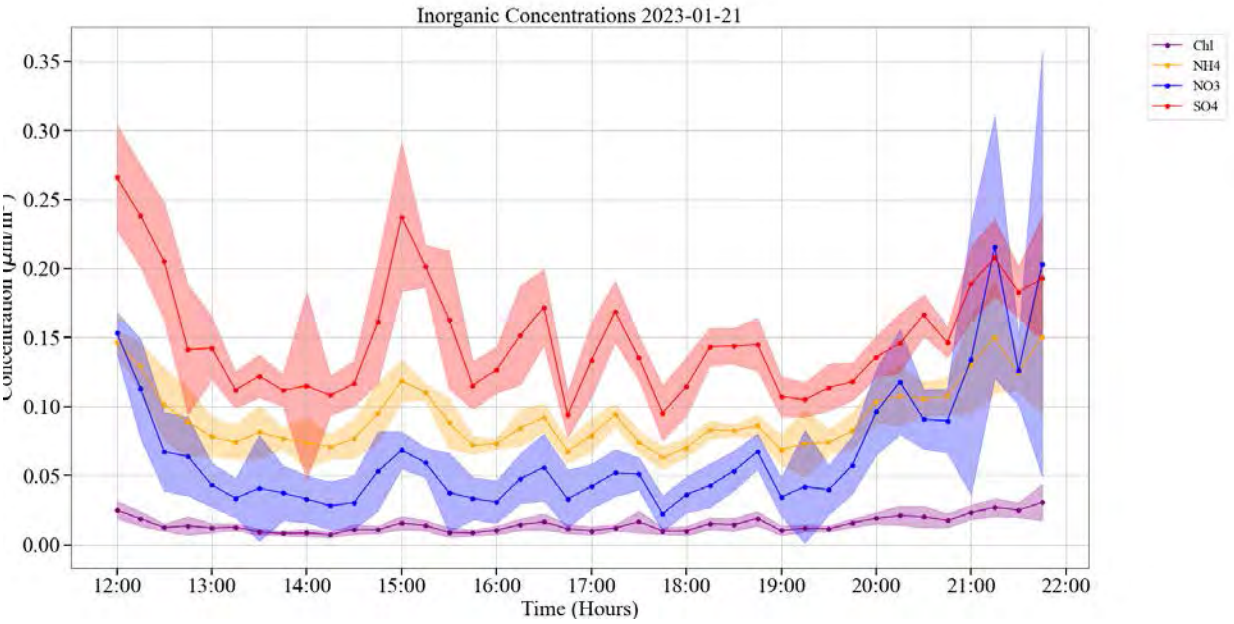

Figure 4.2.4 - Organic Concentration (µg/m^3) January 21, 2023

4.3 CO Data

The carbon monoxide concentrations were also shown below.

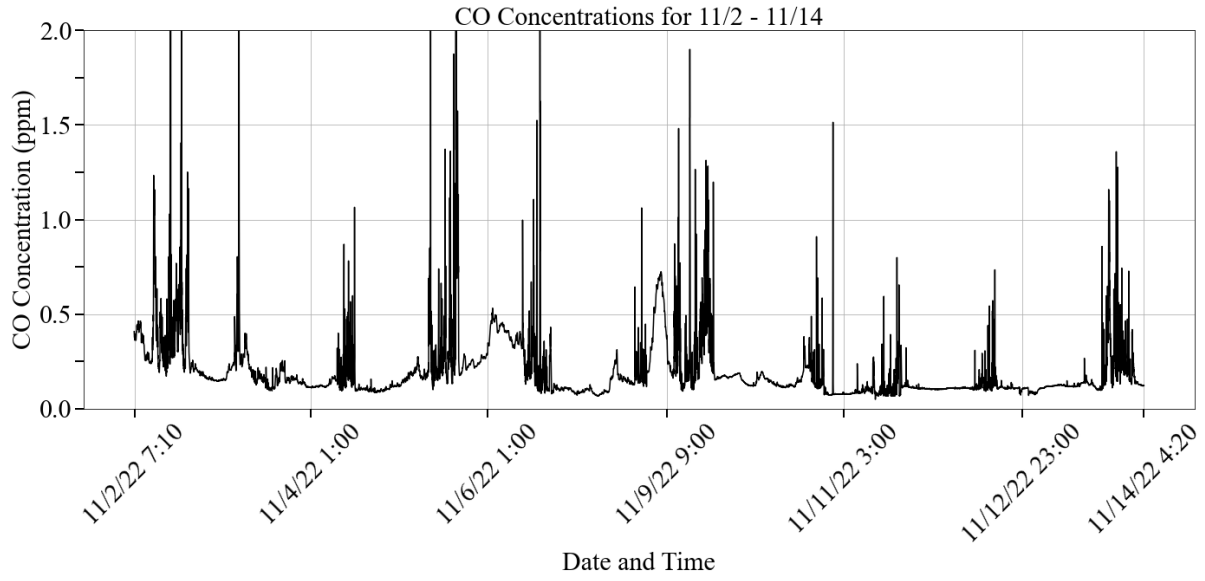

Figure 4.3.1 - CO concentrations for 11/2-11/14

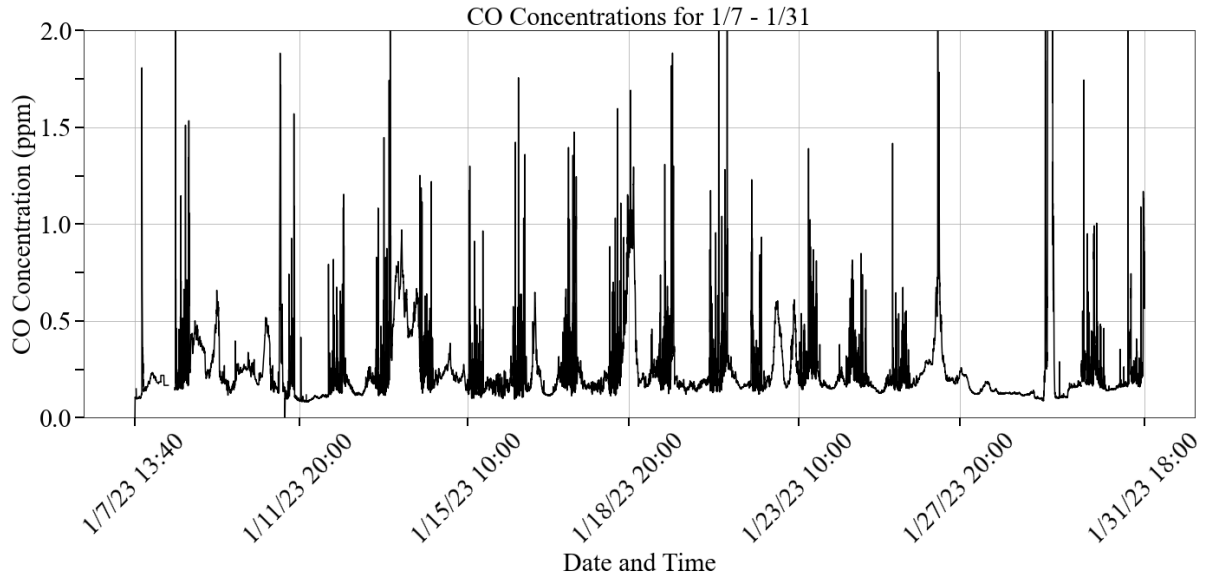

Figure 4.3.2 - CO concentrations for 1/7-1/31

4.4 Comparison of data collected from Vocus NH_4^+ and H^+ modes

To identify any differences between ammonium and PTR ionization modes, we perform 2 different comparisons. First, we compare the average concentration of each VCP measured during the fall and winter for ammonium and PTR (table 4.4 a). Second, we compare the average VCP concentrations measured during both campaigns (table 4.4 b). For these comparisons, only D4-siloxane seems to have a notably higher concentration under ammonium mode. This is the case

both when comparing all the deployment days and when comparing the two seasons. Next steps will be to see how concentrations differ between routes. We will compare the average VCP concentrations for each different route for the fall and winter, and we will compare the average VCP concentrations for each different route for both campaigns.

Table 4.4a: Average VCP concentrations (ppb) for each ionization mode. Averages include both fall and winter.

	Acetone	MEK	D4-siloxane	D5-siloxane	Monoterpenes	PCBTF	Texanol
NH_4^+	6.1111	3.1917	0.0191	0.0147	0.0758	0.0004	0.0001
H^+	2.308	0.5008	0.0004	0.0106	0.1572	0.0019	0.0004

Table 4.4b: Average VCP concentrations (ppb) for each ionization mode. Averages are separate for fall and winter.

	Acetone	MEK	D4-siloxane	D5-siloxane	Monoterpenes	PCBTF	Texanol
Fall NH_4^+	4.5625	0.6567	0.0198	0.0167	0.1187	0.0007	0.0004
Fall H^+	3.7724	0.8411	0.0007	0.0117	0.279	0.003	0.0006
Winter NH_4^+	7.3146	5.1618	0.0187	0.0132	0.0425	0.0002	0
Winter H^+	1.4651	0.3049	0.0003	0.0101	0.0872	0.0013	0.0003

4.5 Seasonal Difference

To identify any differences between the fall and winter campaigns, we perform 2 different comparisons. First, we compare the average concentration of each VCP measured during the fall and winter (4.5a). Second, we compare the average concentration of each VCP:CO ratio measured during the fall and winter (table 4.5 b). For these comparisons, only monoterpenes have a notably higher concentration in the fall deployment. This makes sense considering monoterpenes are emitted from vegetation.

Table 4.5a: Average VCP concentrations (ppb) for fall and winter

	Acetone	MEK	D4-siloxane	D5-siloxane	Monoterpenes	PCBTF	Texanol
Fall	4.1637	0.7498	0.0096	0.0141	0.1996	0.0019	0.0004
Winter	3.6944	2.1289	0.0074	0.0114	0.0699	0.0011	0.0002

Table 4.5b: Average VCP:CO ratios concentrations (ppb/ppb) for fall and winter.

	Acetone :CO	MEK: CO	D4-siloxane: CO	D5-siloxane: CO	Monoterpenes: CO	PCBTF: CO	Texanol: CO
Fall	0.0172	0.0032	0	0.0001	0.0007	0	0
Winter	0.0185	0.0115	0	0.0001	0.0003	0	0

4.6 Comparison of Model Results with Measurements

Organic compounds measured by the mobile platform

The predicted concentrations of CO, acetone, methyl ethyl ketone, and monoterpenes were compared with the geo-tagged 1-min resolution observations made by the mobile platform. The model grid cell where the mobile platform was located at a given time was determined based on the recorded latitude and longitude information. The predicted instantaneous concentrations at the grid cell at the end of two adject hours that brackets the time when the observations were made were weighted to estimate the concentration at time of the observation.

Figure 4.6.1 shows an example of the predicted and observed CO concentrations. The predicted concentrations are significantly lower than the observations. This is expected as the mobile platform is significantly influenced by the tailpipe emissions from on-road vehicles. These high concentrations would not be captured by the model as the predictions represent the average concentrations within a grid cell. However, on all seven days, the lowest values in the observations matched the predictions (e.g., see the panels for November 6 and 10), suggesting that the predictions could reproduce the variations in the regional concentrations when the measurements were not affected by immediate tailpipe emissions.

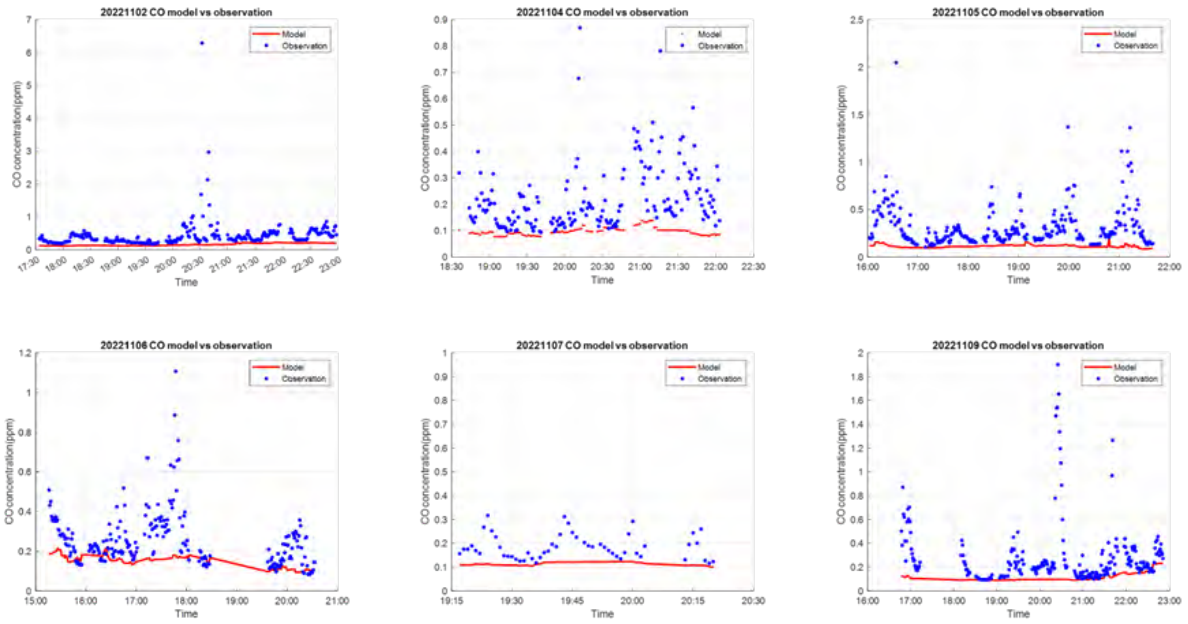

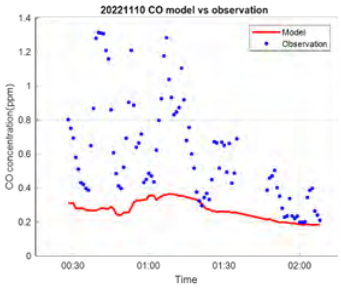

Figure 4.6.1. Predicted (red line) and observed (blue dots) CO concentrations on 7 different days in November 2022. GMT time was used generating these plots.

Figures 4.6.2-4 show that the concentrations of acetone, methyl ethyl ketone, and monoterpene were significantly under predicted on most of the days. Figure 4.6.2 shows that even though the acetone concentrations were underpredicted by approximately a factor of 8, the variations of the concentrations over different days were well captured. However, as shown in Figure 4.6.3, the day-to-day variations of the MEK were not captured well. The model predictions did not show as significant variations as the observed concentrations. The observed ratios of acetone/MEK were generally around 4-7 while the predicted acetone/MEK ratios were mostly less than 2, as shown in Figure 4.6.4.

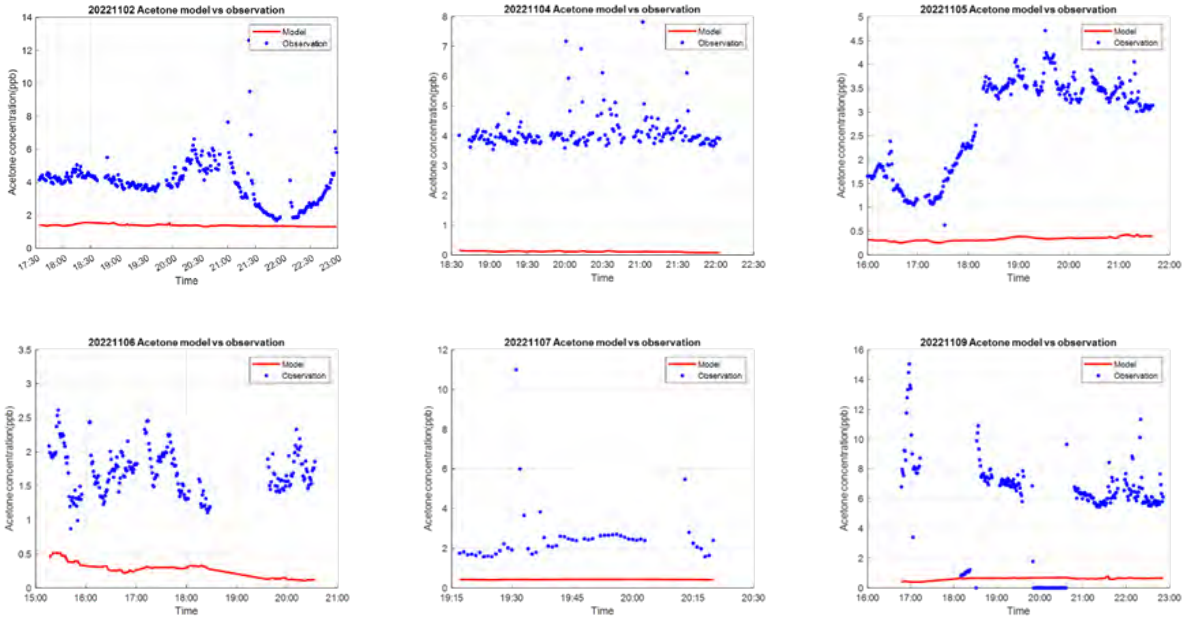

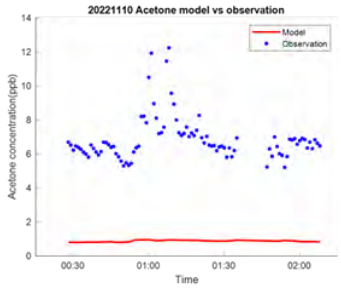

Figure 4.6.2. Predicted (red line) and observed (blue dots) acetone concentrations on 7 different days in November 2022. GMT time was used generating these plots.

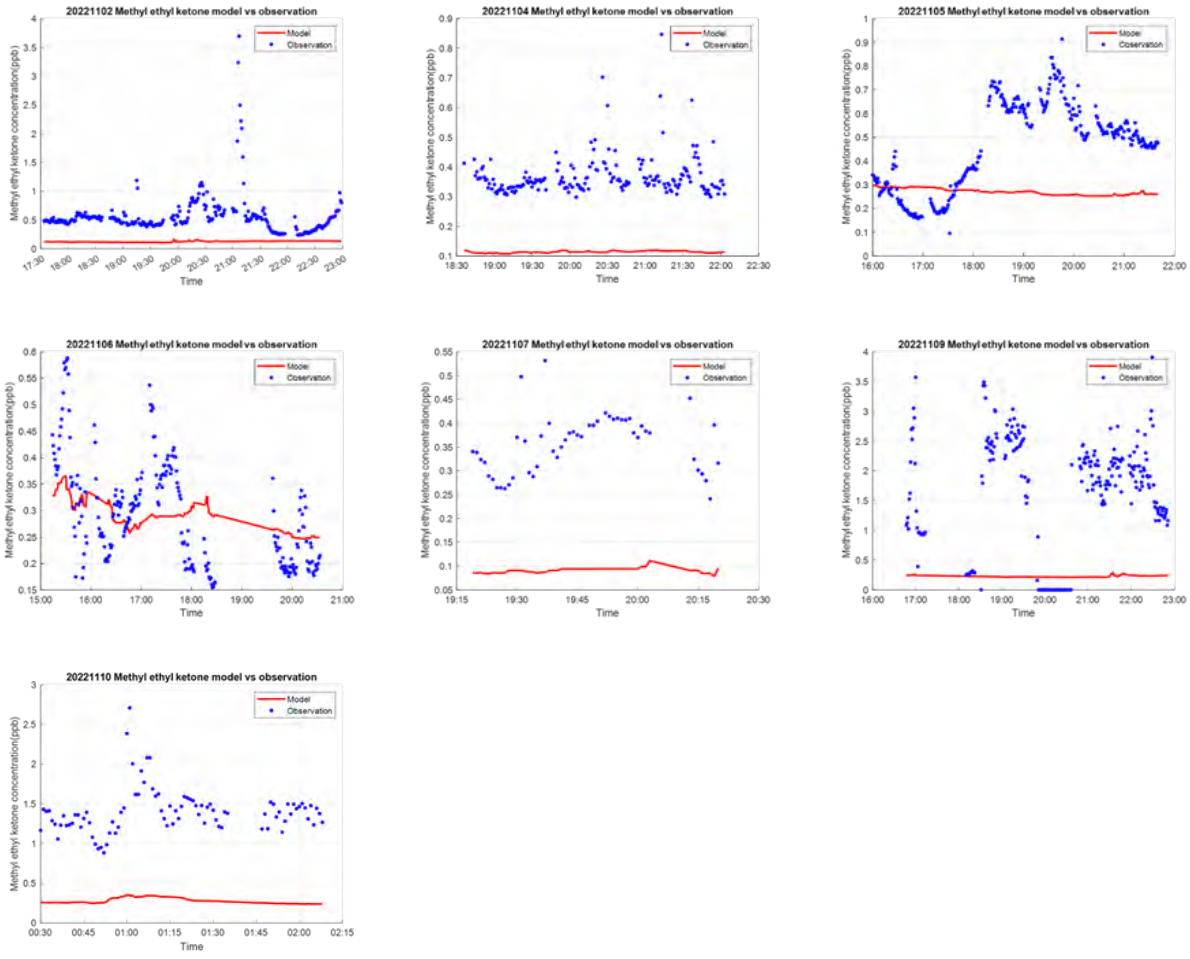

Figure 4.6.3. Predicted (red line) and observed (blue dots) methyl ethyl ketone concentrations on 7 different days in November 2022. GMT time was used generating these plots.

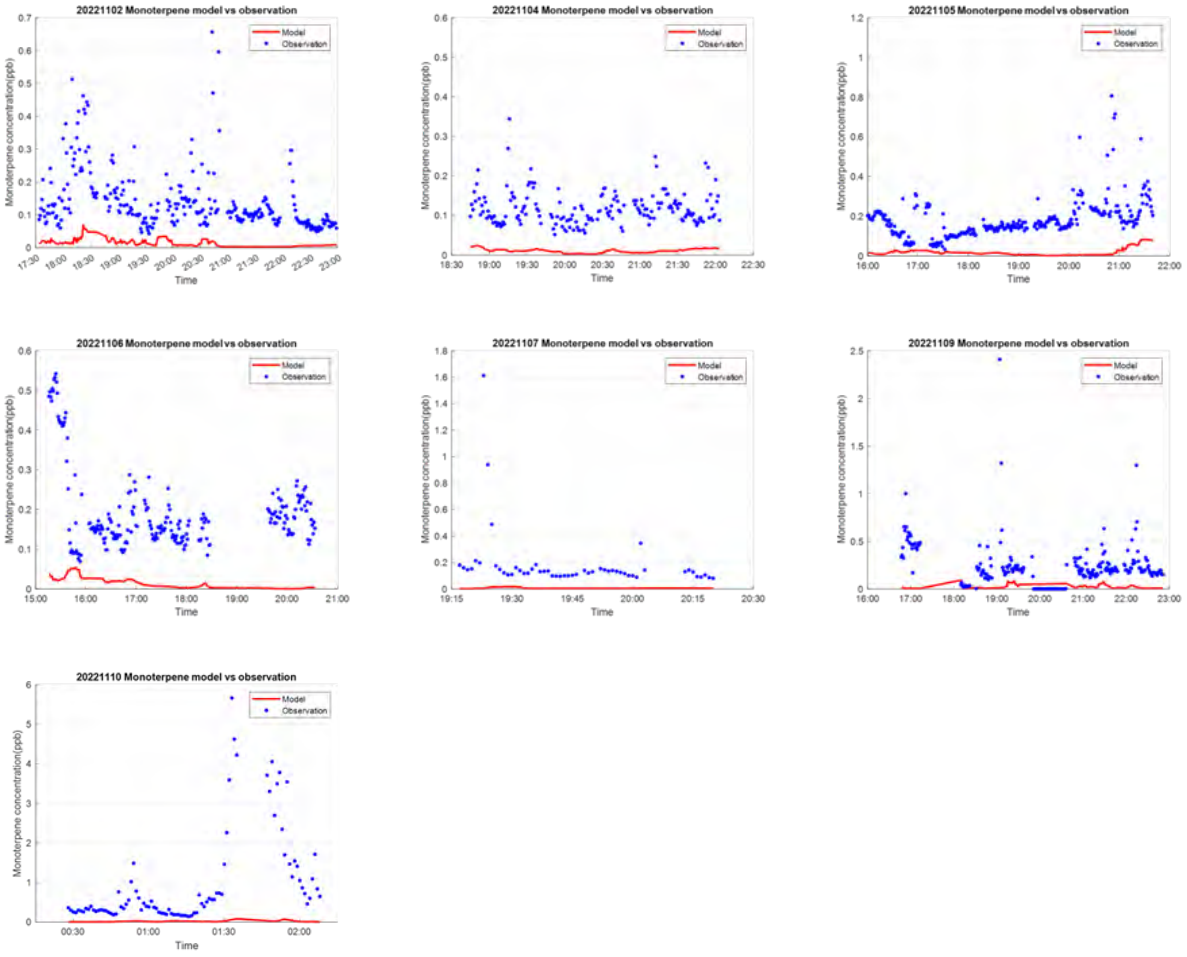

Figure 4.6.4. Predicted (red line) and observed (blue dots) monoterpene concentrations on 7 different days in November 2022. GMT time was used generating these plots. The predicted monoterpene concentrations are the sum of α-pinene, β-pinene, d-limonene, Δ3-carene, and sabinene.

To examine why model results underpredicts some of the key VCP concentration, we have plotted specific modeled and measured acetone and MEK concentrations, as shown below in Figures 4.6.5-4.6.6. A close examination shows that the predictions are accurate at certain times but the acetone concentration can underpredict at other times. On the contrary, the MEK concentration would over predict. Such deviations may be due to the mobile lab being on the road and impacted by other tailpipe emissions. Current chemical transport models do not perform well when analyzing on-road and mobile emissions, which needs further improvements.

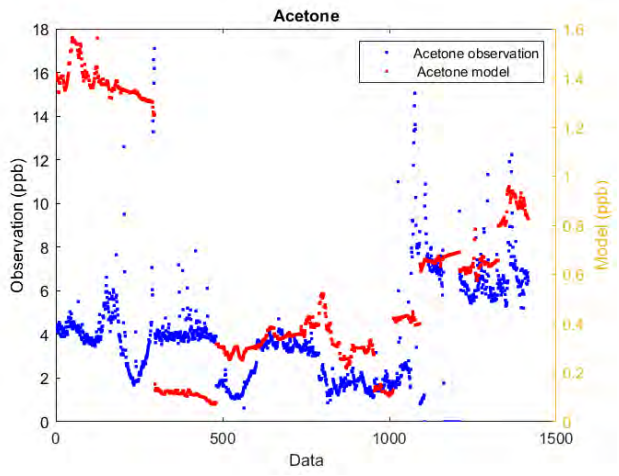

Figure 4.6.5. Predicted and observed acetone concentrations.

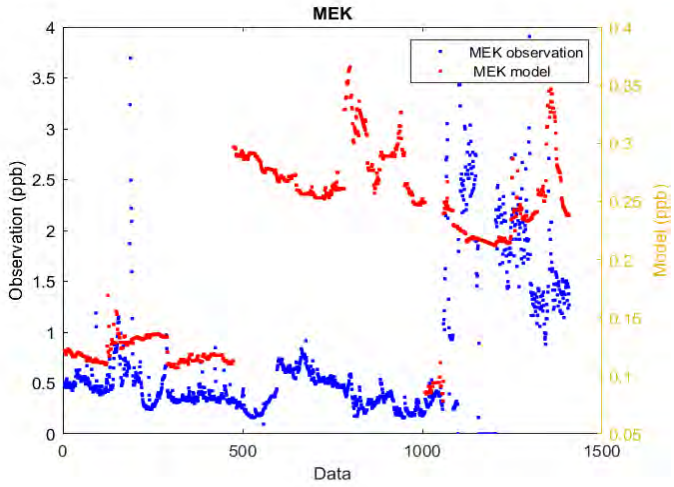

Figure 4.6.6. Predicted and observed methyl ethyl ketone (MEK) concentrations.

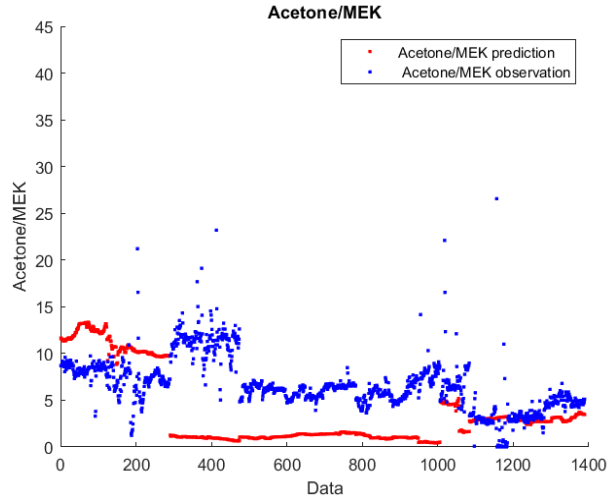

Figure 4.6.7. Calculated values of Acetone concentrations (ppb)/MEK concentrations (ppb) of the model and observation data.

5. Conclusions

During the funded period, we have performed three field campaigns in total, covering three seasons, with the data covering the emission and concentration of VCPs in the summer, fall, and winter. Our results show that the concentrations of seven major VCP groups, namely acetone, PCBTF from solvent-based coating emissions, D5-siloxane from personal care products, D4-siloxane from adhesives and insecticides, monoterpenes from fragrances, methyl ethyl ketone from industrial activities, and texanol from water-based coatings and adhesives. The concentrations of these VCPs range from <0.1 ppt for PCBTF and Texanol to 1-7 ppb for acetone. Monoterpene shows strong seasonal differences in their concentrations, while the concentrations of other types of VCP during different seasons remain to be statistically the same. It is expected that monoterpene has a more drastic seasonal difference due to biogenic emissions during the summer and fall. The similar concentrations and potential emissions of other types of VCPs across different seasons suggest the anthropogenic natural of these compounds. It is also possible that the VCP emissions are lower in the winter but such reduction is offset by a reduced boundary layer height. Further studies are needed to examine the measured boundary layer height and the seasonal emissions of the VCPs. In addition, we also show that certain VCP comprised of a relatively important portion of the total VCPs in Houston based on their absolute concentrations.

Our data further shows that the VCP concentrations measured by the experiments are higher than modeling output, showing that current CAMQ model and inventory may underpredict the ozone formation. Given that VCP has important ozone formation potential in the urban environment, more studies are needed to examine their contribution using TECQ emission inventories. In addition, further studies are needed to examine all other VCPs and their total contribution to the overall VOC concentrations in Houston.